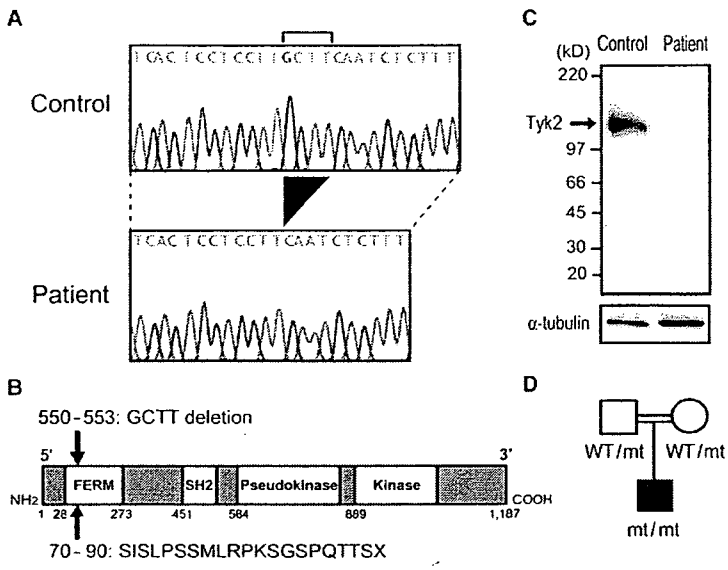


Figure 2. A Homozygous Mutation of the Tyk2 Gene in the Patient

(A) Electropherograms show the part of the Tyk2 cDNA sequences from a control subject and the patient, from which a deletion of four nucleotides, GCTT, was found in the patient.

(B) The structure of Tyk2 is shown schematically, and the mutation is indicated: the 4-nucleotide deletion (above) and the frameshift and truncation of the protein (below).

(C) The Tyk2 protein was undetectable in the patient's T cells. Tyk2 and α-tubulin proteins in the T cells from a healthy control subject and the patient were detected by immunoblotting.

(D) The patient was homozygous for the mutation, and both parents were heterozygous for it. WT, wild-type Tyk2; mt, mutated Tyk2.

the FERM domain, the SH2 domain, and the pseudokinase and kinase domains. Indeed, no Tyk2 protein was detected by immunoblotting with two specific antibodies that recognize different regions of Tyk2 (Figure 2C). Both parents of the patient were apparently healthy and showed normal amounts of serum IgE, but the analysis of genomic DNAs from the parents revealed that both were heterozygous for the same deletion (Figure 2D), establishing that the patient had an autosomal recessive Tyk2 deficiency.

### Tyk2 Is Indispensable for Type I IFN Signaling in Humans

Stimulation of the patient's T cells with various concentrations of IFNα or IFNβ up to 50 ng/ml (equivalent to 10,000 IU/ml) failed to induce tyrosine phosphorylation of not only STAT4 (Figure 1C) but also Jak1, STAT1, STAT2, and STAT3 (Figure 3A and see Figure S1 in the Supplemental Data available online), in contrast to the observation in *Tyk2*$^{-/-}$ mice (Karaghiosoff et al., 2000; Shimoda et al., 2000). Furthermore, no tyrosine phosphorylation of STAT1 and STAT2 was detected at any time points (5, 15, 30, and 60 min) after the treatment with IFNs (Figure S2). Interestingly, the amount of STAT1 protein was reduced in the patient's T cells in accord with the observations in *Tyk2*-deficient mice (Karaghiosoff et al., 2000), whereas those of STAT2, STAT3, and STAT4 proteins appeared unaffected (Figures 1C and 3A, and Figure S3). The patient's T cells displayed a reduced amount of surface IFNAR1 expression (Figure S4). This is consistent with previous observations in a Tyk2-deficient human cell line but in contrast with that in the Tyk2-deficient mice (Gauzzi et al., 1997; Karaghiosoff et al., 2000; Shimoda et al., 2000). Tyk2 has been shown to stabilize IFNAR1 at the cell surface in human cells (Gauzzi et al., 1997; Ragimbeau et al., 2003). Thus, the defect in the type I IFN signaling in the patient's cells could be explained by the absence of Tyk2 accompanied with reduced amounts of STAT1 and IFNAR1.

Consistent with the signaling defects, the transcriptional upregulation of a panel of IFN-inducible genes including NMI and MxA, in response to IFNα or IFNβ, was completely abrogated in PBMCs from the patient (Figure 3B and Figure S5). We further investigated biological consequences of the compromised IFN signaling. The upregulation of HLA class I expression in response to IFNα was not observed in patient PBMCs (Figure 3C). Unexpectedly, the patient's cells displayed a higher basal amount of HLA class I expression than the control cells, suggesting a possible compensatory mechanism to regulate expression in a type I IFN-independent manner under conditions of the Tyk2 deficiency. Even at high concentrations, neither IFNα nor IFNβ produced any antiviral protection against herpes simplex virus (HSV) within the patient B cells (Figures 3D and 3E). Thus, human Tyk2 deficiency showed a complete defect in type I IFN responses under our experimental conditions, in contrast to observations in *Tyk2*$^{-/-}$ mice (Karaghiosoff et al., 2000; Shimoda et al., 2000).

We next examined the response to IFNγ in the patient (Figure 3F). Stimulation with IFNγ upregulated the transcription of two IFNγ-responsive genes, IRF1 and RING4, in PBMCs from the patient and from a healthy control. However, the extent of the induction was much smaller in the patient's PBMC sample, in accord with the impairment of IFNγ signaling reported in *Tyk2*$^{-/-}$ mice (Karaghiosoff et al., 2000).

### Tyk2 Is Critical for IL-23, IL-6, and IL-10 Signaling in Humans

We next examined the response to IL-23 in the patient's cells, because IL-23 shares signaling pathways with IL-12 (Watford et al., 2004). The patient's T cells showed no detectable tyrosine phosphorylation of STAT4 in response to IL-23 even at high concentrations (500 ng/ml) in contrast to T cells from a control subject (Figure 4A). Control T cells secreted IFNγ in response to IL-23 in a dose-dependent manner (Figure 4B) as reported previously (Oppmann et al., 2000). In contrast, the patient's T cells showed no response to IL-23 in IFNγ secretion even though the background amount of

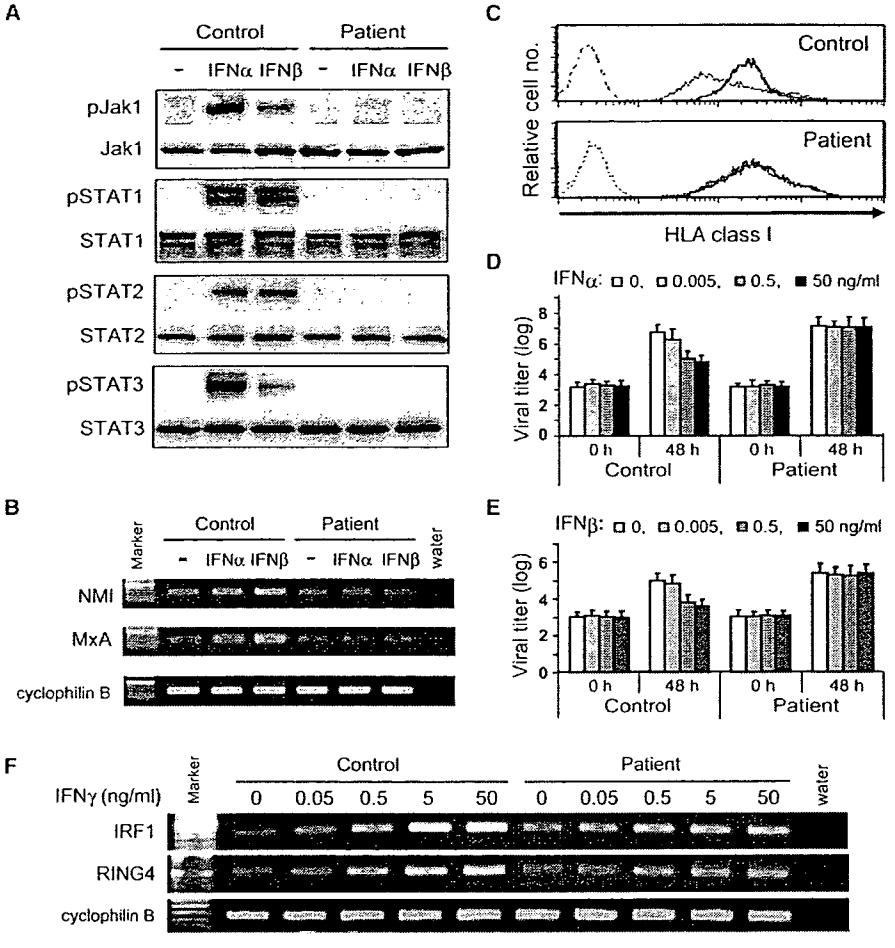


Figure 3. Defects in the Type I and II IFN Signals in the Patient's T Cells

(A) No detectable phosphorylation of the Jak and STAT molecules in the patient's T cells was seen upon stimulation with type I IFN. The indicated proteins (p, phosphorylated form) were detected by immunoblotting after the T cells from a control subject and the patient were stimulated with or without 50 ng/ml (equivalent to 10,000 IU/ml) of IFNα or IFNβ for 15 min.

(B) There was no detectable upregulation of the IFN-inducible gene expression in the patient's cells upon stimulation with type I IFN. The amounts of NMI, MxA, and cyclophilin B transcripts were evaluated by semiquantitative RT-PCR after PBMCs from a control subject and the patient were stimulated or not with IFNα or IFNβ for 2 hr.

(C) No detectable upregulation of HLA class I in the patient's cells upon stimulation with type I IFN. The level of HLA class I on PBMCs from a control subject and the patient was determined with flow cytometry after the cells were cultured with (histograms with thick gray lines) or without (histograms with thin black lines) IFNα for 48 hr. Histograms with dotted lines show the control staining with an isotype-matched mAb.

(D and E) No antiviral activity was detected in the patient's B cells upon stimulation with type I IFN. EBV-transformed B cells from a control subject and the patient were treated for 24 hr with indicated concentrations of IFNα (D) or IFNβ (E) prior to the infection with HSV. The viral titers in culture supernatant of 0 and 48 hr culture were measured by plaque assay with Vero cells. Data are representative of two independent experiments. Error bars are standard deviations.

(F) Impaired response to IFNγ in the patient's cells. The amounts of IRF1, RING4, and cyclophilin B transcripts were evaluated by semiquantitative RT-PCR, after PBMCs from a control subject and the patient were stimulated with the indicated concentration of IFNγ for 2 hr.

IFNγ was slightly higher in the patient's T cells than in the control T cells (Figure 4B). These results indicated that human Tyk2 played an essential role in IL-23 signaling, in accord with observations in the *Tyk2*-deficient mice (Shaw et al., 2003).

It has been demonstrated that Tyk2 is also activated upon stimulation with IL-6 or IL-10 (Ihle, 1995; Stahl et al., 1994). PBMCs from the patient failed to upregulate SOCS3 transcripts in response to IL-6 stimulation (Figure 4C). They secreted IgM when stimulated by infection with Epstein-Barr Virus (EBV), as did those from a healthy control subject. However, further stimulation with IL-6 induced only a little increase in IgM secretion from the patient's PBMCs, although IgM secretion did increase 3 times in the control PBMCs (Figure 4D). The patient's PBMCs had a very poor response to IL-10 stimulation in their induction of SOCS3 (Figure 4E). Moreover, the inhibition of LPS-induced TNFα production by IL-10 was severely impaired in macrophages from the patient (Figure 4F). These results indicated that Tyk2 plays an obligatory role in signaling of IL-6 and IL-10 in humans, in contrast to *Tyk2*$^{-/-}$ mice, which

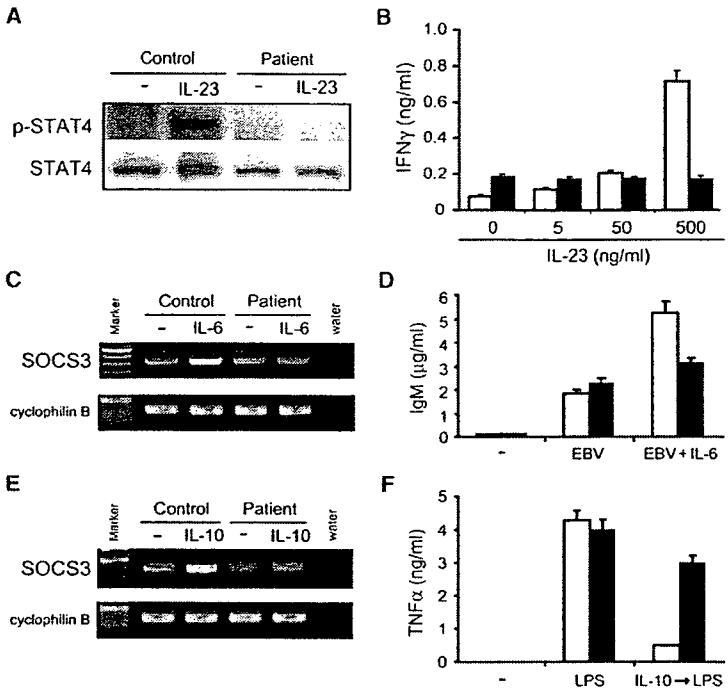


Figure 4. Defects in IL-23, IL-6, and IL-10 Signals in the Patient's Cells

(A) The patient's T cells showed impaired IL-23 signaling. Tyrosine phosphorylated and total STAT4 proteins were detected by immunoblotting after the T cells from a control subject and the patient were stimulated with IL-23 (500 ng/ml) for 15 min.

(B) The patient's T cells showed no substantial response to IL-23 in the IFNγ production. The concentration of IFNγ in culture supernatants was determined by ELISA after the T cells from a control subject and the patient were cultured with the indicated concentrations of IL-23 for 48 hr. White bars indicate a control, and black bars indicate the patient. Error bars are standard deviations.

(C) No detectable upregulation of the SOCS3 gene expression in the patient's cells upon stimulation with IL-6. The amounts of SOCS3 and cyclophilin B transcripts were evaluated by semiquantitative RT-PCR after PBMCs from a control subject and from the patient were stimulated with or without IL-6 for 4 hr.

(D) Little enhancement of IgM secretion in the patient's B cells upon stimulation with IL-6. The concentration of IgM in the culture supernatants was determined by ELISA after PBMCs from a control subject and the patient were cultured for 10 days with or without Epstein-Barr virus (EBV), alone or in combination with IL-6. White bars indicate a control, and black bars indicate the patient. Error bars are standard deviations.

(E) Poor upregulation of the SOCS3 gene expression in the patient's cells upon stimulation with IL-10. The amounts of SOCS3 and cyclophilin B transcripts were evaluated by semiquantitative RT-PCR after PBMCs from a control and the patient were cultured with or without IL-10 for 4 hr.

(F) Poor inhibition of LPS-induced TNFα production by IL-10 in the patient's macrophages. The concentration of TNFα in the culture supernatants was determined by ELISA after macrophages derived from a control subject's and the patient's PBMCs were cultured with or without IL-10 for 24 hr, and then stimulated or not with LPS for 48 hr. White bars indicate a control, and black bars indicate the patient. Error bars are standard deviations. Results are representative of at least three independent experiments.

respond normally to IL-6 (Karaghiosoff et al., 2000; Shimoda et al., 2000). *Tyk2*$^{-/-}$ mice were originally reported to respond normally to IL-10 (Karaghiosoff et al., 2000; Shimoda et al., 2000), while a recent study demonstrates partial impairment in IL-10 signaling (Shaw et al., 2006).

### Imbalance in Th1 and Th2 Differentiation in the Patient

We next examined in vitro the Th1 and Th2 differentiation of T cells from the patient (Figure 5), because the patient displayed Th2-dominant phenotypes such as atopic dermatitis and highly elevated serum IgE. Even under Th1-biased culture conditions, the frequency of IFNγ-producing Th1 cells remained low in the patient's T cells (Figure 5A, middle). On the other hand, their differentiation into IL-4-producing Th2 cells under Th2-biased culture conditions appeared to be accelerated (Figure 5A, right). When cultured for 14 days in the presence of anti-CD3 and IL-2, the patient's T cells showed helper T cell differentiation that was extremely skewed toward Th2, compared with the control T cells (Figure 5B). Naive CD4$^+$ T cells isolated from the patient's PBMCs showed reduced secretion of IFNγ and enhanced secretion of IL-5 and IL-13 as compared to the control T cells when stimulated with anti-CD3 and anti-CD28 (Figure 5C). These results clearly indicated that Tyk2 is critical for the IL-12-induced Th1 differentiation and represses the development of Th2 cells, in accord with the observations in mice (Seto et al., 2003; Shaw et al., 2003).

### Expression of the Intact Tyk2 Gene Rescues the Patient's T Cells from Defects in IL-12 and Type I IFN Signaling

The wild-type Tyk2 gene in a retroviral vector was introduced into activated primary T cells from the patient. The infected T cells acquired the expression of Tyk2 proteins at approximately 70% of the normal amount (Figure 6A). Upon combined stimulation with the IL-12 and IL-18, the infected Tyk-2-expressing cells produced IFNγ, as did T cells from a normal control subject (Figure 6B). In contrast, the patient's T cells infected with virus carrying the empty vector did not produce IFNγ in response to this stimulation, nor did uninfected cells. Furthermore, Tyk2-infected T cells from the patient acquired the ability to upregulate the transcription of MxA in response to IFNα (Figure 6C). A complementary experiment was performed in which human Hela cells were subjected to the knockdown of Tyk2 gene expression with siRNAs. In cells treated with Tyk2-specific siRNAs, the tyrosine phosphorylation of STAT1 and STAT2 in response to IFNα was almost completely abrogated, concomitantly with the suppression of Tyk2 expression, as observed in the patient's cells (Figure S6). These results indicated that the defects in the IL-12 and type I IFN signaling observed in the patient's T cells were caused primarily by the absence of functional Tyk2.

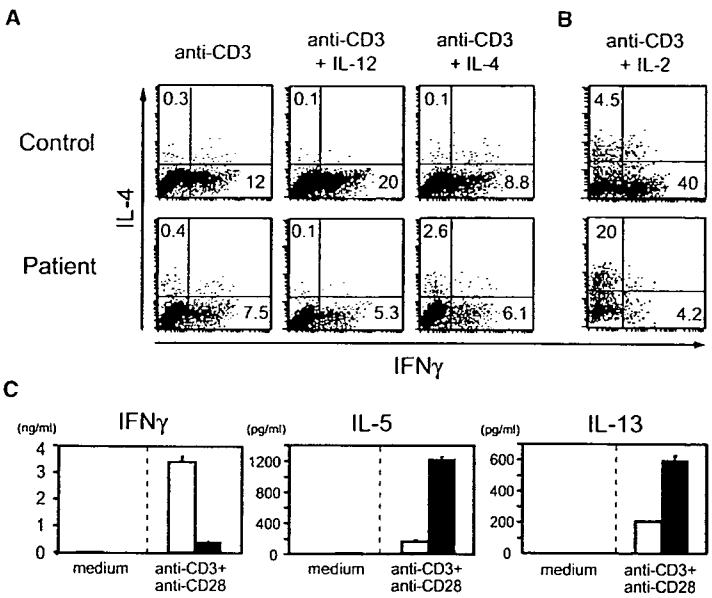


Figure 5. Impaired Th1 and Accelerated Th2 Differentiation in the Patient's T Cells

(A) Intracellular staining with anti-IFNγ and anti-IL-4 was performed after PBMCs from a control subject and the patient were stimulated with immobilized anti-CD3 alone, in combination with IL-12 and anti-IL-4 (Th1-promoting condition) or in combination with IL-4 (Th2-promoting condition) for 5 days. The percentage of IFNγ- or IL-4-producing cells is shown in each panel.

(B) PBMCs from a control subject and the patient were stimulated with immobilized anti-CD3 and IL-2 for 14 days, and intracellular staining was performed as in (A).

(C) Naive $CD4^+$ T cells from a control subject and the patient were stimulated with anti-CD3 and anti-CD28 for 3 days, and the concentration of IFNγ, IL-5, and IL-13 in culture supernatants was measured by ELISA. White bars indicate a control, and black bars indicate the patient. Error bars are standard deviations. Results are representative of at least three independent experiments.

## Discussion

We have identified a human deficiency in Tyk2. Among the four members of the Jak family, Jak3 deficiency was previously reported in human, demonstrating the crucial role of Jak3 in lymphocyte development, in accord with findings in Jak3-deficient mice (Macchi et al., 1995; Nosaka et al., 1995; Park et al., 1995; Russell et al., 1995). The identification of a human Tyk2 deficiency highlighted the obligatory roles of human Tyk2 in multiple cytokine signals involved in innate and acquired immune responses, including type I IFN, IL-6, IL-10, IL-12, and IL-23 signals. Although Tyk2 is ubiquitously expressed (unlike Jak3), the Tyk2 deficiency displayed apparently normal embryogenesis, postnatal growth, and hematopoiesis ,while it resulted in a primary immunodeficiency with clinical manifestations characteristic to HIES, indicating a unique and indispensable role played by Tyk2 in the immune system.

The present study contrasted differences in the stringency of Tyk2 requirement between human and mice. The nonredundant roles of human Tyk2 in multiple cytokine signals in vivo could not be assumed from the studies on mouse Tyk2. The *Tyk2*$^{-/-}$ mice responded normally to IL-6, even though IL-6 activated Tyk2 in vitro. The mice also showed a leaky phenotype in type I IFN responses: a high concentration of IFNα showed antiviral effects and upregulated MHC class I expression in cells from the *Tyk2*$^{-/-}$ mice to an extent comparable to that observed in wild-type mice (Karaghiosoff et al., 2000; Shimoda et al., 2000). This was a sharp contrast to the observation in human Tyk2-deficient fibroblast cell lines. Our results indicated that the discrepancy between these two observations was due to a species difference rather than the difference between primary cells and particular cultured cell lines. We observed no detectable tyrosine phosphorylation of Jak1 in response to type I IFN in the human Tyk2 deficiency, supporting the idea that Tyk2 and Jak1 transphosphorylate each other, and hence both are independently required for the initial activation of IFN signaling. In contrast, in the mouse Tyk2 deficiency, the Jak1 phosphorylation was observed when stimulated with type I IFN, albeit to a lesser extent than in wild-type mice. Thus, Tyk2 is the obligatory requirement for the initiation of type I IFN signaling in human whereas it is redundant in the initiation and might function as an amplifier of signaling in mice. This also appears to be the case in the IL-12 signaling. *Tyk2*$^{-/-}$ mice showed compromised signaling and biological effects in response to IL-12 (Karaghiosoff et al., 2000; Seto et al., 2003; Shaw et al., 2003; Shimoda et al., 2000), but the impairment was less drastic than that observed in IL-12 receptor-deficient mice (Wu et al., 1997).

The in vitro findings of defects in multiple cytokine signals due to the Tyk2 deficiency appeared to account for the complex clinical manifestations of the patient investigated in the present study. First, the susceptibility to viral infection could be attributed to the defect in IFN signaling. Indeed, even a high titer of type I IFNs did not show any protective effect against herpes simplex virus in the patient's cells, unlike in *Tyk2*$^{-/-}$ mice (Karaghiosoff et al., 2000; Shimoda et al., 2000). Interestingly, the response to type II IFN (IFNγ) stimulation was also impaired in the patient's T cells, albeit to a lesser extent, even though Tyk2 has not been assigned to the type II IFN signaling pathway. The partial impairment of IFNγ signaling could be explained, at least in part, by the reduced amounts of STAT1 protein or by the observation that IFNγ signaling depends on constitutive subthreshold type I IFN signaling (Takaoka et al., 2000). Thus, the type II IFN response is reduced but not absent in the Tyk2 deficiency in contrast to its complete lack in the STAT1 deficiency (Dupuis et al., 2003), even though the type I IFN response is absent in both deficiencies. This could account for the apparently milder phenotype of the Tyk2 deficiency in viral infections, compared to the lethal phenotype of the STAT1 deficiency. It remains

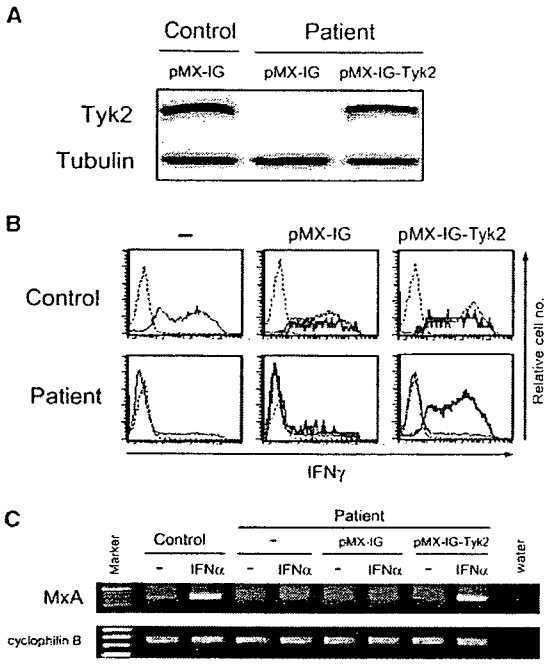


Figure 6. Transduction of the Intact Tyk2 Gene Rescued the Patient's T Cells from Defects in the IL-12 and Type I IFN Signals

(A) Reconstitution of Tyk2 in the patient's T cells. T cells from the patient and a control subject were infected with either the empty retroviral vector (pMX-IG) or the Tyk2 cDNA-containing vector (pMX-IG-Tyk2). The protein expression of Tyk2 and tubulin in GFP$^+$-infected cells were detected by immunoblotting.

(B) Retrovirus-mediated Tyk2 transfer restored the IFNγ production in response to IL-12 and IL-18 in the patient's T cells. The production of IFNγ was detected by intracellular staining with an IFNγ mAb in uninfected and infected T cells after stimulation with IL-12 and IL-18 for 48 hr. Histograms with thick gray lines show the staining profile of GFP$^+$-infected cells, and those with thin black lines show the staining profile of GFP$^-$ uninfected cells. Histograms with dotted lines show the control staining with an isotype-matched mAb.

(C) Retrovirus-mediated Tyk2 transfer restored the upregulation of IFN-inducible gene expression in response to IFNα in the patient's T cells. The amounts of MxA and cyclophilin B transcripts were evaluated by semiquantitative RT-PCR after stimulation of the indicated T cells with IFNα for 2 hr. Results are representative of at least three independent experiments.

to be determined whether the type III IFN (IL-28 and IL-29) signaling is defective in the Tyk2 deficiency.

Second, the susceptibility of the patient to infection with intracellular bacteria, such as mycobacteria and salmonella, could be explained by the defect in IL-12 signaling, as seen in IL-12Rβ1 deficiency (Altare et al., 1998; de Jong et al., 1998). The differentiation into Th1 cells, which are important for the elimination of these bacteria, was severely impaired in the patient's T cells, even under culture conditions that strongly promote the differentiation of Th1 cells. Given that type I IFNs promote Th1 differentiation in humans and not in mice, the defect in the IFN signal might also account in part for the failure of Th1 differentiation in this patient. The susceptibility of Tyk2 knockout mice to infection of intracellular bacterial has not been reported, but a natural mutant strain B10.Q/J, which is susceptible to toxoplasma infection and resistant to induction of autoimmune arthritis, was reported to carry Tyk2 mutation (Shaw et al., 2003). Mice deficient for IL-23 showed the susceptibility to Klebsiella pneumonia owing to their impairment in IL-17 production by T cells (Happel et al., 2005). Therefore, the patient's susceptibility to extracellular bacteria might be explained at least in part by the defect in IL-23 signaling.

Third, the high amount of serum IgE and the atopic dermatitis-like skin inflammation in the patient could be due to the accelerated Th2 differentiation. Indeed, the Tyk2 deficiency was shown to accelerate Th2-mediated allergic airway inflammation in mice (Seto et al., 2003). In a previous report, enhanced Th2 differentiation was not observed in an IL-12Rβ1 deficiency, although the Th1 differentiation was severely impaired (Wood et al., 2005). Thus, the defect in IL-12 signaling does not account for the abnormally accelerated Th2 differentiation in the Tyk2-deficient patient. PBMCs and macrophages from the patient showed a severe signaling defect in the IL-10 pathway. IL-10 has been reported to suppress the differentiation of both Th1 and Th2 cells, so the defect in the IL-10 pathway might explain, at least in part, the accelerated Th2 differentiation under conditions in which Th1 differentiation was defective as observed in mice deficient for both IL-10 and IL-12 (Hoffmann et al., 2000).

The patient investigated in the present study had been clinically diagnosed as HIES, fulfilling the criteria for the diagnosis according to the NIH scoring system (Grimbacher et al., 1999b). HIES is a primary immunodeficiency with unknown etiology, characterized typically by high serum IgE amounts, recurrent staphylococcal skin abscesses, and pneumonia with pneumatocele formation (Grimbacher et al., 2005). While most cases of HIES are sporadic, families displaying autosomal dominant (AD) or autosomal recessive (AR) inheritance have been reported (Grimbacher et al., 1999a; Renner et al., 2004). In most sporadic and AD cases, these clinical manifestations are part of a multisystem disorder including abnormalities of the soft tissue, skeletal, and dental systems (Grimbacher et al., 1999a). In contrast, patients with AR-HIES lack skeletal and dental involvement and lung cyst formation and suffer from fungal and viral infections such as herpes simplex and molluscum contagiosum (Renner et al., 2004). According to this classification, the present case could be categorized into the AR-HIES. It is notable that the infection with intracellular bacteria experienced by the present case has not been frequently observed in HIES patients, even though three cases with mycobacterial infection were reported in the literatures (Grimbacher et al., 1999a; Metin et al., 2004; Pasic et al., 1998). Therefore, we would like to propose that the present case represents a subset of the AR-HIES. The whole picture of HIES including its etiology has not yet drawn clearly, so further genetic analyses of HIES is needed to evaluate this proposal and define the Tyk2 deficiency as either a variant of HIES or a distinct disease entity. In either case, the present study highlighted a requisite and nonredundant role played by Tyk2 in the innate and acquired immune responses in human.

## Experimental Procedures

### Patient

This study was approved by the institutional review board at the Tokyo Medical and Dental University. Written informed consent

was obtained from all the subjects studied. The patient investigated in this study is a 22-year-old Japanese male with a history of infantile atopic dermatitis starting from 1 month of age and recurrent infections, such as otitis media, sinusitis, pneumonias, and skin abscesses, starting from 12 months of age. At 22 months, he developed BCG lymphadenitis. Histological examination revealed paucibacillary, well-circumscribed granulomas with epithelioid and giant multinucleated cells, as observed in the human IL-12Rβ1 deficiency (Altare et al., 1998; de Jong et al., 1998). The immunological work-up performed at this occasion revealed mild eosinophilia (700–800/mm$^3$) and high serum IgE (2100 IU/ml) with normal amounts of other Ig classes and subclasses. All other laboratory data examined were within the normal range, including complement components, the oxidative burst of granulocytes, the number and the size of platelets, lymphocyte subpopulations, and their proliferative responses to mitogens. The patient's illness was tentatively diagnosed as HIES though he did not show any apparent skeletal abnormality. Thereafter, in addition to infections with bacteria including *Staphylococcus aureus*, he recurrently suffered from viral and fungal infections, such as molluscum contagiosum, herpes simplex infection of skin and mucosa, and oral candidiasis. At 15 years of age, the patient developed severe non-typhi salmonella gastroenteritis leading to sepsis. According to the HIES scoring system (Grimbacher et al., 1999b), the patient gained 48 points; 10 in IgE titers, 8 in skin abscess, 8 in pneumonia, 3 in eosinophil count, 4 in newborn rash, 4 in eczema, 2 in upper respiratory infection, 1 in oral candidiasis, 4 in other serious infections, and 4 in fatal infection.

### Antibodies and Cytokines

The mAbs for the N-terminal region (aa 46–258) of human Tyk2, IL-12Rβ1, IL-12Rβ2, IκBα, IL-4, and IFNγ were purchased from BD Pharmingen, and the CD3 mAb (OKT3) was from Janssen Pharmaceutical. The Ab for the C-terminal region of Tyk2 (C-8) was from Santa Cruz. Rabbit antibodies for Jak1, STAT1, STAT2, STAT3, and STAT4 and their phosphorylated forms were purchased from Cell Signaling. Anti-IFNAR1 was from R&D Systems. HRP-conjugated rabbit anti-mouse and goat anti-rabbit antibodies were from Calbiochem, and mouse anti-α-tubulin was from Sigma-Aldrich. Recombinant human IL-4, IL-12, IFNα, IFNβ, IFNγ, and GM-CSF were purchased from Peprotech, recombinant human IL-2 was from Shionogi, and IL-18 was from MBL.

### Isolation and Culture of T Cells and Macrophages from PBMCs

Heparinized blood samples were obtained from the patient and from healthy age-matched control subjects. PBMCs were isolated from blood samples through density gradient centrifugation via Histopaque-1077 (Sigma-Aldrich). For T cell activation, PBMCs were cultured with 5 μg/ml plate-bound CD3 mAb and 300 U/ml IL-2 in RPMI 1640 (Sigma-Aldrich) containing 10% fetal bovine serum (FBS), 50 μM 2-mercaptoethanol (Life Technologies), 2% L-glutamine, 1 mM sodium pyruvate, 0.1 mM nonessential amino acids, and 1% penicillin-streptomycin. CD4$^+$ T cells were enriched with immunomagnetic beads (BD Pharmingen) with more than 98% purity. After 14 days of culture, more than 98% of the cells from both the patient and control subjects were effector memory T cells (CD45RO$^+$CCR7$^-$). Naive CD4$^+$ T cells were purified by removing CD45RO$^+$ cells from CD4$^+$ T cells by immunomagnetic beads (BD Pharmingen) with more than 90% purity. To obtain macrophages, PBMCs were cultured for 2 hr, and the adherent cells were further cultured with 10 ng/ml GM-CSF for 7 days as described (Hart et al., 1995). All the experiments were performed at least three times with three different controls.

### Construction of Retroviral Vectors and Infection of Cells

The retroviral vector pMX-IRES-GFP-Tyk2 was constructed by inserting the Tyk2 cDNA into the BamHI and NotI sites of the pMX-IRES-GFP vector (a gift from T. Kitamura) (Nosaka et al., 1999). Infectious retroviral particles were generated with the Plat-GP cell line (a gift from T. Kitamura and H. Miyoshi). Retroviral supernatant stocks were produced by culturing the producer cells at 37°C for 72 hr. For the infection, PBMCs were stimulated in culture with 5 μg/ml plate-bound CD3 mAb and 300 IU/ml IL-2. Cells (1 × 10$^6$/ml) were then spin-infected with the retroviral supernatant at 32°C for 30 min. The transduction procedure was repeated on days 2 and 3. The efficiency of infection was approximately 3% as judged by the frequency of GFP$^+$ cells.

### Tyk2 Knockdown

RNA interference for Tyk2 was designed with the aid of the online software from Invitrogen. The sequences of siRNA sense strands (5′ → 3′) were as follows: Tyk2 siRNA1, CCCAGAGAUGCAAGCCU GAUGCUAU, and Tyk2 siRNA2, CCAUUCUGAAGACAGUCCAUGA GAA. Hela cells were grown in DMEM supplemented with 10% FBS. Transfection of the cells with siRNAs was performed with Lipofectamine-RNAiMAX reagent (Invitrogen). 48 hr after transfection, the cells were treated with IFNα (50 ng/ml) for 15 min before lysis. Lysates were analyzed by immunoblotting with the antibodies indicated.

### RT-PCR and Direct Sequence Analysis

Extraction of total RNA, cDNA synthesis, PCR, and semiquantitative RT-PCR were performed as previously described (Minegishi et al., 1999a). PCR primers were designed as follows: Tyk2, sense, 5′-TTGCTTGAGTTGACACAGGGAGCT-3′, antisense, 5′-TCTCTAGAC AGGAGTAAGGCACAC-3′; STAT4, sense, 5′-CTGGGACCTGTGCTG AGAGAGC-3′, antisense, 5′-ACTTTTTCATTTGCTTCCTT-3′; NMI, sense, 5′-TTAAGGAGCATTCGCCAGAT-3′, antisense, 5′-TTCGAGC TCACTTGAAACGA-3′, MxA, sense, 5′-GAGGTGCAGGAGAACAG CTC-3′, antisense 5′-CTCCTCATACTGGCTGCACA-3′; cyclophilin B, sense, 5′-GCCCAAAGTCACCGTCAAGG-3′, antisense, 5′-GGAA GCGCTCACCGTAGATG-3′; IRF1, sense, 5′-GCTGGGACATCAACA AGGAT-3′, antisense, 5′-GTGGAAGCATCCGGTACACT-3′; RING4, sense, 5′-AGGGCTGGCTGGCTGCTTTGA-3′, antisense, 5′-ACGTG GCCCATGGTGTTGTTAT-3′; and SOCS3, sense, 5′-TTCAGCTCCA AGAGCGAGTA-3′, antisense, 5′-CGGAGTAGATGTAATATGGCTC-3′. Sequencing was performed with an ABI Prism dRhodamine Terminator kit and analyzed with an ABI Prism 310 DNA Sequencer (Perkin-Elmer Applied Biosystems).

### Stimulation of Cells with Cytokines and the Measurement of Cytokine and Ig Production

Cells were stimulated for the indicated time in culture with PMA (40 nM), ionomycin (0.5 μg/ml), IL-12 (10 ng/ml), IL-18 (50 ng/ml), IFNα (50 ng/ml), IFNβ (50 ng/ml), IL-6 (10 ng/ml), or IL-10 (100 ng/ml). The concentration of IFNγ in the culture supernatants was determined by ELISA (BD-PharMingen) according to the manufacturer's instructions, after the cells (1 × 10$^6$/ml) were cultured in 96-well plates at 37°C for 24 hr with or without stimulation. The concentration of TNFα in the culture supernatants was determined by ELISA (BD-PharMingen), after the cells (1 × 10$^5$/well) were cultured in 96-well plates at 37°C for 48 hr with or without stimulation. The measurement of IgM secretion from Epstein-Barr virus-infected B cells was determined by ELISA as previously described (Minegishi and Conley, 2001). To evaluate helper T cell differentiation in vitro, PBMCs were cultured for 5 days with immobilized anti-CD3 alone or in combination with IL-12 (10 ng/ml) and anti-IL-4 (10 μg/ml) to promote Th1 differentiation, or in combination with IL-4 (20 ng/ml) to promote Th2 differentiation, or the PBMCs were cultured for 14 days with immobilized anti-CD3 and IL-2 (300 IU/ml). Alternatively, naive CD4$^+$ T cells were cultured with immobilized anti-CD3 and soluble anti-CD28 for 3 days. The concentration of IFNγ, IL-5, and IL-13 in the culture supernatants was determined by ELISA (BD Pharmingen).

### Flow Cytometric Analysis

The surface immunophenotype was analyzed as described (Minegishi et al., 1999a). For cytokine intracellular staining, cells were restimulated with PMA and ionomycin in the presence of 2 μM of monensin for 5 hr, followed by fixation and cytoplasmic staining with FITC- or PE-conjugated mAbs specific for the indicated cytokines. An irrelevant FITC- or PE-conjugated IgG1 mAb was used as the negative control.

### Immunoblotting and Immunoprecipitation

Cells were washed and cultured for 18 hr in starvation medium consisting of RPMI 1640 and 1% FBS. Cells were then stimulated at 37°C for 15 min with medium alone, 10 ng/ml IL-12, 50 ng/ml IL-18, 50 ng/ml IFNα, or 50 ng/ml IFNβ. After the stimulation, the cells

were lysed on ice for 30 min in lysis buffer containing 1% Triton X-100, 50 mM Tris (pH 8.0), 150 mM NaCl, 2 mM EDTA, 2 μg/ml aprotinin, 100 μg/ml PMSF, 1 mM sodium orthovanadate, and 1 mM NaF. The cell lysates were subjected to SDS-PAGE, followed by electrotransfer to PVDF membranes and immunoblotting with the indicated antibodies.

### Antiviral Activity Assay

EBV-transformed B cells were pretreated with or without 0.005, 0.5, 50 ng/ml IFNα or IFNβ for 24 hr, and then infected with HSV ($10^3$ plaque-forming units/ml). The viral titers in culture supernatants were determined at the indicated time points by plaque assay with Vero cells.

### Supplemental Data

Six Supplemental Figures can be found with this article online at http://www.immunity.com/cgi/content/full/25/5/745/DC1/.

### Acknowledgments

We appreciate the willingness of the patient and the parents to participate in this research study. This work is supported by Grants-in-Aid 16616004, 17047013, and 18659299 from the Japanese Ministry of Education, Culture, Sports, Science, and Technology and Grants-in-Aid 2212131 and 2211932 from the Japanese Ministry of Health, Labor, and Welfare.

Received: May 3, 2006
Revised: June 27, 2006
Accepted: September 19, 2006
Published online: November 9, 2006

### References

Alexander, W.S., and Hilton, D.J. (2004). The role of suppressors of cytokine signaling (SOCS) proteins in regulation of the immune response. Annu. Rev. Immunol. *22*, 503–529.

Altare, F., Durandy, A., Lammas, D., Emile, J.F., Lamhamedi, S., Le Deist, F., Drysdale, P., Jouanguy, E., Doffinger, R., Bernaudin, F., et al. (1998). Impairment of mycobacterial immunity in human interleukin-12 receptor deficiency. Science *280*, 1432–1435.

Bacon, C.M., McVicar, D.W., Ortaldo, J.R., Rees, R.C., O'Shea, J.J., and Johnston, J.A. (1995). Interleukin 12 (IL-12) induces tyrosine phosphorylation of JAK2 and TYK2: differential use of Janus family tyrosine kinases by IL-2 and IL-12. J. Exp. Med. *181*, 399–404.

Casanova, J.L., and Abel, L. (2004). The human model: a genetic dissection of immunity to infection in natural conditions. Nat. Rev. Immunol. *4*, 55–66.

Conley, M.E., Rohrer, J., Rapalus, L., Boylin, E.C., and Minegishi, Y. (2000). Defects in early B-cell development: comparing the consequences of abnormalities in pre-BCR signaling in the human and the mouse. Immunol. Rev. *178*, 75–90.

de Jong, R., Altare, F., Haagen, I.A., Elferink, D.G., Boer, T., van Breda Vriesman, P.J., Kabel, P.J., Draaisma, J.M., van Dissel, J.T., Kroon, F.P., et al. (1998). Severe mycobacterial and *Salmonella* infections in interleukin-12 receptor-deficient patients. Science *280*, 1435–1438.

Dupuis, S., Jouanguy, E., Al-Hajjar, S., Fieschi, C., Al-Mohsen, I.Z., Al-Jumaah, S., Yang, K., Chapgier, A., Eidenschenk, C., Eid, P., et al. (2003). Impaired response to interferon-α/β and lethal viral disease in human STAT1 deficiency. Nat. Genet. *33*, 388–391.

Fieschi, C., Bosticardo, M., de Beaucoudrey, L., Boisson-Dupuis, S., Feinberg, J., Santos, O.F., Bustamante, J., Levy, J., Candotti, F., and Casanova, J.L. (2004). A novel form of complete IL-12/IL-23 receptor β1 deficiency with cell surface-expressed nonfunctional receptors. Blood *104*, 2095–2101.

Firmbach-Kraft, I., Byers, M., Shows, T., Dalla-Favera, R., and Krolewski, J.J. (1990). tyk2, prototype of a novel class of non-receptor tyrosine kinase genes. Oncogene *5*, 1329–1336.

Gauzzi, M.C., Barbieri, G., Richter, M.F., Uze, G., Ling, L., Fellous, M., and Pellegrini, S. (1997). The amino-terminal region of Tyk2 sustains the level of interferon alpha receptor *1*, a component of the interferon α/β receptor. Proc. Natl. Acad. Sci. USA *94*, 11839–11844.

Grimbacher, B., Holland, S.M., Gallin, J.I., Greenberg, F., Hill, S.C., Malech, H.L., Miller, J.A., O'Connell, A.C., and Puck, J.M. (1999a). Hyper-IgE syndrome with recurrent infections—an autosomal dominant multisystem disorder. N. Engl. J. Med. *340*, 692–702.

Grimbacher, B., Schaffer, A.A., Holland, S.M., Davis, J., Gallin, J.I., Malech, H.L., Atkinson, T.P., Belohradsky, B.H., Buckley, R.H., Cossu, F., et al. (1999b). Genetic linkage of hyper-IgE syndrome to chromosome 4. Am. J. Hum. Genet. *65*, 735–744.

Grimbacher, B., Holland, S.M., and Puck, J.M. (2005). Hyper-IgE syndromes. Immunol. Rev. *203*, 244–250.

Happel, K.I., Dubin, P.J., Zheng, M., Ghilardi, N., Lockhart, C., Quinton, L.J., Odden, A.R., Shellito, J.E., Bagby, G.J., Nelson, S., and Kolls, J.K. (2005). Divergent roles of IL-23 and IL-12 in host defense against *Klebsiella pneumoniae*. J. Exp. Med. *202*, 761–769.

Hart, P.H., Jones, C.A., and Finlay-Jones, J.J. (1995). Monocytes cultured in cytokine-defined environments differ from freshly isolated monocytes in their responses to IL-4 and IL-10. J. Leukoc. Biol. *57*, 909–918.

Hoffmann, K.F., Cheever, A.W., and Wynn, T.A. (2000). IL-10 and the dangers of immune polarization: excessive type 1 and type 2 cytokine responses induce distinct forms of lethal immunopathology in murine schistosomiasis. J. Immunol. *164*, 6406–6416.

Ihle, J.N. (1995). Cytokine receptor signalling. Nature *377*, 591–594.

Karaghiosoff, M., Neubauer, H., Lassnig, C., Kovarik, P., Schindler, H., Pircher, H., McCoy, B., Bogdan, C., Decker, T., Brem, G., et al. (2000). Partial impairment of cytokine responses in Tyk2-deficient mice. Immunity *13*, 549–560.

Liu, K.D., Gaffen, S.L., and Goldsmith, M.A. (1998). JAK/STAT signaling by cytokine receptors. Curr. Opin. Immunol. *10*, 271–278.

Macchi, P., Villa, A., Giliani, S., Sacco, M.G., Frattini, A., Porta, F., Ugazio, A.G., Johnston, J.A., Candotti, F., O'Shea, J.J., et al. (1995). Mutations of Jak-3 gene in patients with autosomal severe combined immune deficiency (SCID). Nature *377*, 65–68.

Metin, A., Uysal, G., Guven, A., Unlu, A., and Ozturk, M.H. (2004). Tuberculous brain abscess in a patient with hyper IgE syndrome. Pediatr. Int. *46*, 97–100.

Minegishi, Y., and Conley, M.E. (2001). Negative selection at the pre-BCR checkpoint elicited by human mu heavy chains with unusual CDR3 regions. Immunity *14*, 631–641.

Minegishi, Y., Coustan-Smith, E., Wang, Y.H., Cooper, M.D., Campana, D., and Conley, M.E. (1998). Mutations in the human λ5/14.1 gene result in B cell deficiency and agammaglobulinemia. J. Exp. Med. *187*, 71–77.

Minegishi, Y., Coustan-Smith, E., Rapalus, L., Ersoy, F., Campana, D., and Conley, M.E. (1999a). Mutations in Igα (CD79a) result in a complete block in B-cell development. J. Clin. Invest. *104*, 1115–1121.

Minegishi, Y., Rohrer, J., Coustan-Smith, E., Lederman, H.M., Pappu, R., Campana, D., Chan, A.C., and Conley, M.E. (1999b). An essential role for BLNK in human B cell development. Science *286*, 1954–1957.

Muller, M., Briscoe, J., Laxton, C., Guschin, D., Ziemiecki, A., Silvennoinen, O., Harpur, A.G., Barbieri, G., Witthuhn, B.A., Schindler, C., et al. (1993). The protein tyrosine kinase JAK1 complements defects in interferon-α/β and -γ signal transduction. Nature *366*, 129–135.

Neubauer, H., Cumano, A., Muller, M., Wu, H., Huffstadt, U., and Pfeffer, K. (1998). Jak2 deficiency defines an essential developmental checkpoint in definitive hematopoiesis. Cell *93*, 397–409.

Nosaka, T., van Deursen, J.M., Tripp, R.A., Thierfelder, W.E., Witthuhn, B.A., McMickle, A.P., Doherty, P.C., Grosveld, G.C., and Ihle, J.N. (1995). Defective lymphoid development in mice lacking Jak3. Science *270*, 800–802.

Nosaka, T., Kawashima, T., Misawa, K., Ikuta, K., Mui, A.L., and Kitamura, T. (1999). STAT5 as a molecular regulator of proliferation, differentiation and apoptosis in hematopoietic cells. EMBO J. *18*, 4754–4765.

Oppmann, B., Lesley, R., Blom, B., Timans, J.C., Xu, Y., Hunte, B., Vega, F., Yu, N., Wang, J., Singh, K., et al. (2000). Novel p19 protein

engages IL-12p40 to form a cytokine, IL-23, with biological activities similar as well as distinct from IL-12. Immunity *13*, 715–725.

O'Shea, J.J., Gadina, M., and Schreiber, R.D. (2002). Cytokine signaling in 2002: new surprises in the Jak/Stat pathway. Cell *109* (*Suppl*), S121–S131.

Parganas, E., Wang, D., Stravopodis, D., Topham, D.J., Marine, J.C., Teglund, S., Vanin, E.F., Bodner, S., Colamonici, O.R., van Deursen, J.M., et al. (1998). Jak2 is essential for signaling through a variety of cytokine receptors. Cell *93*, 385–395.

Park, S.Y., Saijo, K., Takahashi, T., Osawa, M., Arase, H., Hirayama, N., Miyake, K., Nakauchi, H., Shirasawa, T., and Saito, T. (1995). Developmental defects of lymphoid cells in Jak3 kinase-deficient mice. Immunity *3*, 771–782.

Pasic, S., Lilic, D., Pejnovic, N., Vojvodic, D., Simic, R., and Abinun, M. (1998). Disseminated Bacillus Calmette-Guerin infection in a girl with hyperimmunoglobulin E syndrome. Acta Paediatr. *87*, 702–704.

Ragimbeau, J., Dondi, E., Alcover, A., Eid, P., Uze, G., and Pellegrini, S. (2003). The tyrosine kinase Tyk2 controls IFNAR1 cell surface expression. EMBO J. *22*, 537–547.

Renner, E.D., Puck, J.M., Holland, S.M., Schmitt, M., Weiss, M., Frosch, M., Bergmann, M., Davis, J., Belohradsky, B.H., and Grimbacher, B. (2004). Autosomal recessive hyperimmunoglobulin E syndrome: a distinct disease entity. J. Pediatr. *144*, 93–99.

Rodig, S.J., Meraz, M.A., White, J.M., Lampe, P.A., Riley, J.K., Arthur, C.D., King, K.L., Sheehan, K.C., Yin, L., Pennica, D., et al. (1998). Disruption of the Jak1 gene demonstrates obligatory and nonredundant roles of the Jaks in cytokine-induced biologic responses. Cell *93*, 373–383.

Russell, S.M., Tayebi, N., Nakajima, H., Riedy, M.C., Roberts, J.L., Aman, M.J., Migone, T.S., Noguchi, M., Markert, M.L., Buckley, R.H., et al. (1995). Mutation of Jak3 in a patient with SCID: essential role of Jak3 in lymphoid development. Science *270*, 797–800.

Seto, Y., Nakajima, H., Suto, A., Shimoda, K., Saito, Y., Nakayama, K.I., and Iwamoto, I. (2003). Enhanced Th2 cell-mediated allergic inflammation in Tyk2-deficient mice. J. Immunol. *170*, 1077–1083.

Shaw, M.H., Boyartchuk, V., Wong, S., Karaghiosoff, M., Ragimbeau, J., Pellegrini, S., Muller, M., Dietrich, W.F., and Yap, G.S. (2003). A natural mutation in the Tyk2 pseudokinase domain underlies altered susceptibility of B10.Q/J mice to infection and autoimmunity. Proc. Natl. Acad. Sci. USA *100*, 11594–11599.

Shaw, M.H., Freeman, G.J., Scott, M.F., Fox, B.A., Bzik, D.J., Belkaid, Y., and Yap, G.S. (2006). Tyk2 negatively regulates adaptive Th1 immunity by mediating IL-10 signaling and promoting IFN-gamma-dependent IL-10 reactivation. J. Immunol. *176*, 7263–7271.

Shimoda, K., Kato, K., Aoki, K., Matsuda, T., Miyamoto, A., Shibamori, M., Yamashita, M., Numata, A., Takase, K., Kobayashi, S., et al. (2000). Tyk2 plays a restricted role in IFNα signaling, although it is required for IL-12-mediated T cell function. Immunity *13*, 561–571.

Stahl, N., Boulton, T.G., Farruggella, T., Ip, N.Y., Davis, S., Witthuhn, B.A., Quelle, F.W., Silvennoinen, O., Barbieri, G., Pellegrini, S., et al. (1994). Association and activation of Jak-Tyk kinases by CNTF-LIF-OSM-IL-6 βreceptor components. Science *263*, 92–95.

Takaoka, A., Mitani, Y., Suemori, H., Sato, M., Yokochi, T., Noguchi, S., Tanaka, N., and Taniguchi, T. (2000). Cross talk between interferon-γ and -α/β signaling components in caveolar membrane domains. Science *288*, 2357–2360.

Velazquez, L., Fellous, M., Stark, G.R., and Pellegrini, S. (1992). A protein tyrosine kinase in the interferon α/β signaling pathway. Cell *70*, 313–322.

Watford, W.T., Hissong, B.D., Bream, J.H., Kanno, Y., Muul, L., and O'Shea, J.J. (2004). Signaling by IL-12 and IL-23 and the immunoregulatory roles of STAT4. Immunol. Rev. *202*, 139–156.

Wood, P.M., Fieschi, C., Picard, C., Ottenhoff, T.H., Casanova, J.L., and Kumararatne, D.S. (2005). Inherited defects in the interferon-gamma receptor or interleukin-12 signalling pathways are not sufficient to cause allergic disease in children. Eur. J. Pediatr. *164*, 741–747.

Wu, C., Ferrante, J., Gately, M.K., and Magram, J. (1997). Characterization of IL-12 receptor β1 chain (IL-12Rβ1)-deficient mice: IL-12Rβ1 is an essential component of the functional mouse IL-12 receptor. J. Immunol. *159*, 1658–1665.

# DELAYED SEPARATION OF THE UMBILICAL CORD IN TWO SIBLINGS WITH INTERLEUKIN-1 RECEPTOR-ASSOCIATED KINASE 4 DEFICIENCY: RAPID SCREENING BY FLOW CYTOMETER

HIDETOSHI TAKADA, MD, PHD, HIDETO YOSHIKAWA, MD, PHD, MASUE IMAIZUMI, MD, PHD, TARO KITAMURA, MD, PHD, JUNJI TAKEYAMA, MD, PHD, SATORU KUMAKI, MD, PHD, AKIHIKO NOMURA, MD, PHD, AND TOSHIRO HARA, MD, PHD

**We describe 2 siblings who had interleukin-1 receptor-associated kinase 4 deficiency with a novel mutation in exon 2. They had delayed separation of the umbilical cord. The flow cytometric analysis of monocytic intracellular tumor necrosis factor-α production in response to lipopolysaccharide may be a useful method to screen for the disease.** ***(J Pediatr 2006;148:546-8)***

The Toll-like receptors (TLRs) play important roles in the recognition of microbial conserved molecular patterns [1] and activate signaling pathways via interleukin-1 receptor-associated kinases (IRAKs) to induce inflammatory responses against the pathogens.[2] TLR2 and TLR4 play pivotal roles in the recognition of *Streptococcus pneumoniae* or its components including lipoteichoic acid and pneumolysin.[3,4] In 5 patients reported with IRAK4 deficiency, extracellular pyogenic bacterial infections occurred recurrently early in life but became less frequent with age.[5-8] On the other hand, 2 siblings with IRAK4 deficiency had lethal pneumococcal meningitis.[9] We report 2 siblings with a novel mutation in *IRAK4* gene, who had delayed separation of the umbilical cord. Here we present a rapid screening method for this immunodeficiency.

## CASE REPORT

A 2-year-old boy was admitted to the hospital because of fever from that morning and generalized seizure. He was the first child of non-consanguineous healthy parents. He had delayed separation of the umbilical cord in the neonatal period. He received surgical manipulation for persistent urachus 39 days after birth, and his umbilical cord was resected at that time. He had pneumococcal meningitis accompanied with pneumococcal arthritis of the left hip joint when he was 1 year old. He received bacillus Calmette-Guerin, measles, polio, and rubella live vaccinations with no adverse effect. He did not receive *S pneumoniae* vaccination.

On admission, he had a temperature of 39° C and was somnolent. The white blood cell count was 8900 cells/mm$^3$ (neutrophil, 90%). The cerebrospinal fluid was cloudy, and gram-positive bacilli were observed microscopically. *S pneumoniae* was isolated from culture. Serum C-reactive protein concentration was 10.32 mg/dL. Serum levels of immunoglobulins, C3, C4, and $CH_{50}$ were within normal limits. Flow cytometric analysis revealed normal expression levels of CD11a, CD11b, CD11c, and CD18 on neutrophils. The superoxide production test and phagocytic activity of neutrophils were within normal ranges. Three hours after admission, the patient suddenly had development of hypotension, anuria, and convulsions. Despite intensive therapies against meningitis, severe brain edema and disseminated intravascular coagulation led to death 25 days after admission.

## METHODS

For exon 2-5 of *IRAK4* gene, genomic DNA was amplified for each exon by polymerase chain reaction, and direct sequencing was performed with an ABI PRISM 3100 Genetic Analyzer (Perkin-Elmer, Foster City, CA). The primer pairs were as

| | | | |
|---|---|---|---|
| IRAK4 | Interleukin-1 receptor–associated kinase 4 | TLR | Toll-like receptor |
| LPS | lipopolysaccharide | | |

See related article, p 549

From the Department of Pediatrics, Graduate School of Medical Sciences, Kyushu University, the Departments of Neurology, Hematology and Oncology, and Clinical Pathology, Miyagi Children's Hospital, and the Department of Pediatric Oncology, Institute of Development, Aging and Cancer, Tohoku University.

Submitted for publication Aug 12, 2005; last revision received Oct 20, 2005; accepted Dec 2, 2005.

Reprint requests: Hidetoshi Takada, MD, PhD, Department of Pediatrics, Graduate School of Medical Sciences, Kyushu University, 3-1-1, Maidashi, Higashi-ku, Fukuoka 812-8582, Japan. Tel: +81-92-642-5421, Fax: +81-92-642-5435, E-mail: takadah@pediatr.med.kyushu-u.ac.jp

0022-3476/$ - see front matter



10.1016/j.jpeds.2005.12.015

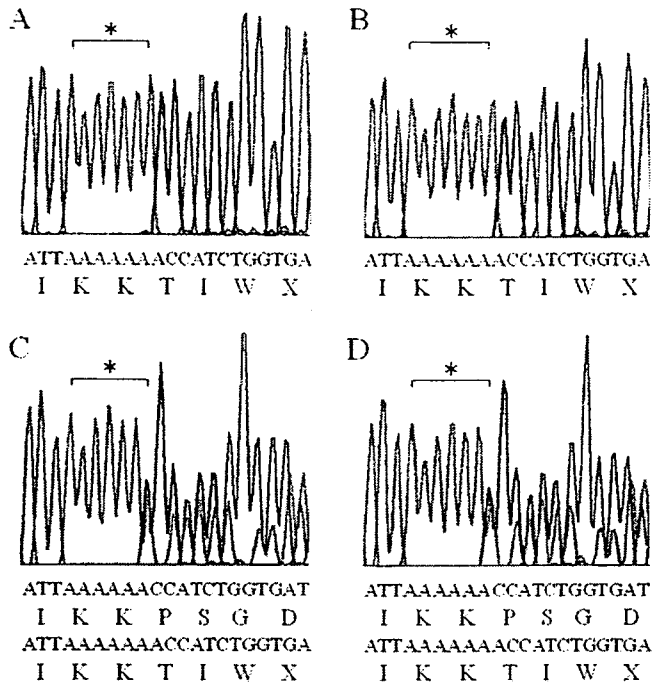


**Figure 1.** Genetic analysis of IRAK4 deficiency. Exon 2 of *IRAK4* gene was amplified with polymerase chain reaction, and direct sequencing was performed. Homozygous mutation c.167_172insA was observed in exon 2 of patients (**A**, elder brother, **B**, younger brother). Both parents were heterozygotes of this mutation (**C**, father, **D**, mother). *Asterisk* indicates site of mutation. Available in color at www.jpeds.com.

follows: exon 2: 5′-GGTATAATCAGTTGCTGACATT-TCATA-3′ and 5′-TCCTCCATAGTGGAGAGGTTT-3′; exon 3: 5′-CAGAACCGTGAGCCAAATTA-3′ and 5′-TGAAAGAAAGGGACTCTCAAATG-3′; exon 4: 5′-CCAACCTGTAGAAACTGGAATG-3′ and 5′-GT-GCCTGTGATTGCTGCAC-3′; and exon 5: 5′-TG-GTTTTATCTTCTCTCATCTTGTC-3′ and 5′-TT-TTTCTAGGGGTAGGGTCCA-3′. For the remaining coding regions of IRAK4 gene, cDNA was amplified and sequenced. The primer pair was 5′-TCATTTTATGAAT-TGAAGAATGTCAC-3′ and 5′-AACCCATGCTTTA-ATAACCACTGTC-3′.

Peripheral blood cells were stimulated with LPS for 4 hours, and intracellular TNF-$\alpha$ staining was performed using the Fastimmune Intracellular Staining System (BD Bioscience Pharmingen, San Diego, CA). The analysis gate was set for monocytes by side scatter and CD14 expression. This study was performed according to the Regional Committee of Ethics for Human Research at Kyushu University.

## RESULTS

Sequencing analysis of the *IRAK4* gene revealed homozygous 1 base pair insertion in exon 2 (c.167_172insA), which led to the generation of premature stop codon (Figure 1, *A*). His parents were heterozygotes of the mutation (Figure 1, *C* and *D*). We analyzed *IRAK4*gene of the younger brother, whose umbilical cord was separated 34 days after birth and found the same homozygous mutation in *IRAK4* gene (Figure 1, *B*). He had no apparent infection at 5 months after birth. Interleukin-6 (IL-6) and TNF-$\alpha$ production was almost completely defective in mononuclear cells 24 hours after stimulation with lipoteichoic acid (for the stimulation of TLR2), LPS (TLR4), poly:IC (TLR3), and IL-1$\beta$ (IL-1 receptor) (data not shown). This result prompted us to analyze the usefulness of the flow cytometric analysis of monocytic intracellular cytokine production in response to LPS as a screening method of this disease. As shown in Figure 2, TNF-$\alpha$ production was profoundly impaired in the IRAK4-deficient patient compared with healthy control subjects and patients with chronic granulomatous disease or hyperimmunoglobulinemia E syndrome.

## DISCUSSION

IRAK4 is a kinase that plays a crucial role in the TLRs and IL-1 receptor (IL-1R) signaling. Ligand binding to these receptors triggers the recruitment of the adaptor protein myeloid differentiation factor 88 (MyD88), IRAK4, and then IRAK1, which allows IRAK4 to phosphorylate IRAK1, recruit TRAF6, and activate downstream signal transduction.[10] In this report, the elder brother had lethal pneumococcal meningitis, which demonstrates that IRAK4 deficiency is one of the primary immunodeficiency syndromes that can lead to severe, life-threatening bacterial infections.[9]

Delayed separation of umbilical cord was observed in both patients, which has not been reported previously. The precise mechanism of cord separation is not known, but drying, infarction, collagenase activity, necrosis, and granulocyte influx may all influence the time at which it occurs.[11] In primary immunodeficiency syndromes, it is observed in leukocyte adhesion deficiency type 1 (LAD type1), E-selectin deficiency, and Ras-related C3 botulinum toxin substrate 2 (Rac2) deficiency[12]. Although it is possible that persistent urachus was responsible for this manifestation in the elder brother,[11] the younger brother had no urachal anomalies. Although it does not seem to be observed in all patients with IRAK4 deficiency,[6] the lack of inflammatory responses may play a role in this manifestation.

It has become clarified that various pathogens can cause severe infections in IRAK4 deficiency.[8] In addition, IRAK4-deficient patients lack specific abnormalities in usual laboratory examinations. Therefore it may be difficult to select the patients for further evaluation of IRAK4 deficiency among those who have bacterial infections with various frequencies and severities. The flow cytometric analysis of monocytic intracellular TNF-$\alpha$ production (Figure 2) is a rapid, easy, and cost-effective method for screening for IRAK4 deficiency. Furthermore, it may help to find and clarify other unknown diseases with defects in TLR/IL-1R signaling molecules.

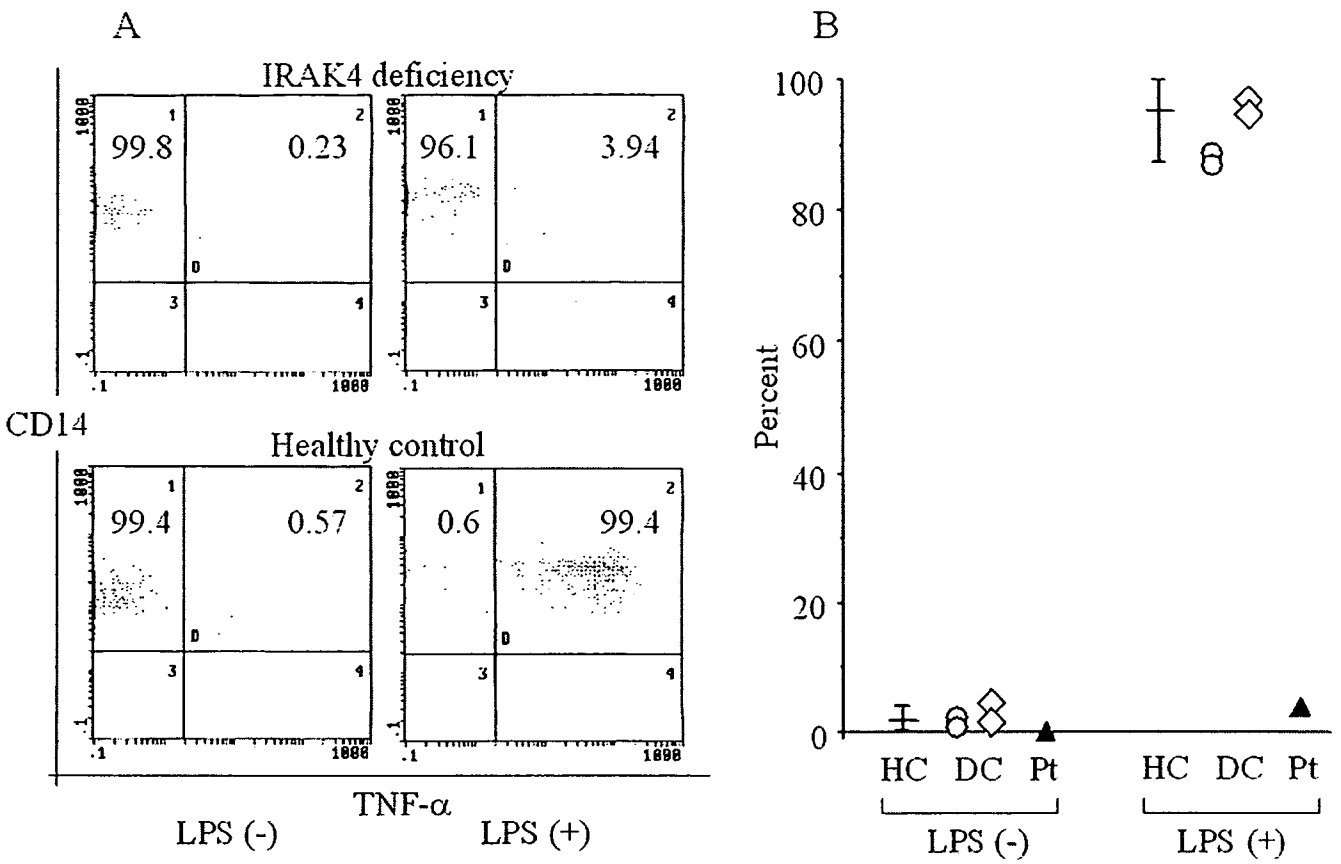


**Figure 2.** Flow cytometric analysis of intracellular TNF-α production of monocytes in response to LPS. Intracellular staining for TNF-α was performed, and its expression in monocytes was analyzed by use of flow cytometry. Representative data of intracellular TNF-α staining **(A)** and percentage of TNF-α–producing cells in monocytes **(B)** with and without LPS stimulation were shown. *HC,* Age-matched healthy control subjects; *DC,* disease controls (*open circles,* patients with CGD; *open squares,* patients with HIES), *Pt,* younger brother (IRAK4 deficiency patient). *Horizontal bars* indicate median and range in age-matched 9 healthy control subjects.

## REFERENCES


1. Medzhitov R. Toll-like receptors and innate immunity. Nat Rev Immunol 2001;1:135-45.
2. Takeda K, Kaisho T, Akira S. Toll-like receptors. Annu Rev Immunol 2003;21:335-76.
3. Yoshimura A, Lien E, Ingalls RR, Tuomanen E, Dziarski R, Golenbock D. Recognition of Gram-positive bacterial cell wall components by the innate immune system occurs via Toll-like receptor 2. J Immunol 1999;163:1-5.
4. Malley R, Henneke P, Morse SC, Cieslewicz MJ, Lipsitch M, Thompson CM, Kurt-Jones E, Paton JC, Wessels MR, Golenbock DT. Recognition of pneumolysin by Toll-like receptor 4 confers resistance to pneumococcal infection. Proc Natl Acad Sci USA 2003;100:1966-71.
5. Picard C, Puel A, Bonnet M, Ku CL, Bustamante J, Yang K, et al. Pyogenic bacterial infections in humans with IRAK-4 deficiency. Science 2003;299:2076-9.
6. Medvedev AE, Lentschat A, Kuhns DB, Blanco JC, Salkowski C, Zhang S, et al. Distinct mutations in IRAK-4 confer hyporesponsiveness to lipopolysaccharide and interleukin-1 in a patient with recurrent bacterial infections. J Exp Med 2003;198:521-31.
7. Day N, Tangsinmankong N, Ochs H, Rucker R, Picard C, Casanova JL, et al. Interleukin receptor-associated kinase (IRAK-4) deficiency associated with bacterial infections and failure to sustain antibody responses. J Pediatr 2004;144:524-6.
8. Chapel H, Puel A, von Bernuth H, Picard C, Casanova JL. Shigella sonnei meningitis due to interleukin-1 receptor-associated kinase-4 deficiency: first association with a primary immune deficiency. Clin Infect Dis 2005;40:1227-31.
9. Enders A, Pannicke U, Berner R, Henneke P, Radlinger K, Schwarz K, et al. Two siblings with lethal pneumococcal meningitis in a family with a mutation in interleukin-1 receptor-associated kinase 4. J Pediatr 2004;145:698-700.
10. Janssens S, Beyaert R. Functional diversity and regulation of different interleukin-1 receptor associated kinase (IRAK) family members. Mol Cell 2003;11:293-302.
11. Razvi S, Murphy R, Shlasko E, Cunningham-Rundles C. Delayed separation of the umbilical cord attributable to urachal anomalies. Pediatrics 2001;108:493-4.
12. Rosenzweig SD, Uzel G, Holland SM. Phagocytic disorders. In: Stiem ER, Ochs HD, Winkelstein JA, editors. Immunologic disorders in infants and children. 5th ed. Philadelphia: Elsevier; 2004. p. 618-51.

# Selective utilization of nonhomologous end-joining and homologous recombination DNA repair pathways during nervous system development

Kenji E. Orii*, Youngsoo Lee*, Naomi Kondo†, and Peter J. McKinnon*‡

*Department of Genetics and Tumor Cell Biology, St. Jude Children's Research Hospital, Memphis, TN 38105; and †Department of Pediatrics, Gifu University School of Medicine, Gifu 501-1194, Japan

Edited by James E. Cleaver, University of California, San Francisco, CA, and approved May 9, 2006 (received for review March 28, 2006)

**The repair of DNA double-strand breaks (DSBs) occurs via nonhomologous end-joining (NHEJ) or homologous recombination (HR). These mechanistically distinct pathways are critical for maintenance of genomic integrity and organismal survival. Although inactivation of either pathway leads to embryonic lethality, here we show selective requirements for each DNA DSB repair pathway at different stages of mammalian nervous system development. DNA damage-induced apoptosis resulting from inactivation of HR (Xrcc2 deficiency) only occurred in proliferating neural precursor cells, whereas disruption of NHEJ (DNA ligase IV deficiency) mainly affected differentiating cells at later developmental stages. Therefore, these data suggest that NHEJ is dispensable for a substantial portion of early development because DSB repair during this period utilizes HR. Moreover, DNA damage-induced apoptosis required the ataxia telangiectasia mutated (Atm) kinase after disruption of NHEJ, but not HR, during neurogenesis. However, embryonic lethality arising from disruption of either repair pathway was rescued by loss of p53 and resulted in specific tumor types reflective of the particular DSB repair pathway inactivated. Thus, these data reveal distinct tissue- and cell-type requirements for each DNA DSB repair pathway during neural development and provide insights for understanding the contributions of DNA DSB responses to disease.**

ataxia telangiectasia mutated | DNA double strand-break | tumorigenesis | neurogenesis | genomic instability

Nonhomologous end-joining (NHEJ) and homologous recombination (HR) are mechanistically distinct DNA repair pathways that ensure the repair of DNA double-strand breaks (DSBs). These pathways differ in their DNA template requirements and the fidelity of the repair process. HR requires a group of RAD51-related proteins that includes XRCC2 to ensure high fidelity DNA repair by using an undamaged homologous DNA template to replace an adjacent damaged one (1, 2). In contrast, NHEJ facilitates direct modification and ligation of the two DNA ends present at the DSB. Efficient NHEJ requires Ku heterodimers (Ku70 and Ku80), DNA-PK catalytic subunit (PKcs), DNA ligase IV (Lig4), and XRCC4 (3, 4). Additionally, other components are also required, amongst which may be Artemis and the recently described XRCC4-binding factor XLF/Cernunnos (5, 6). Whereas NHEJ can participate in repair during all cell cycle phases, HR is functionally important from late synthesis (S) phase to mitosis (7), although there is likely to be cross-talk and cooperation between these two pathways (8–10). Components of each pathway are ubiquitously expressed, and it is assumed that both pathways are competent for and participate in DNA repair, although NHEJ is generally considered the predominant pathway for repairing DSBs in mammalian cells (4). Thus, together, NHEJ and HR provide an effective means of responding to DNA DSBs and act to prevent the accumulation of damaged DNA. However, delineating distinct roles and the functional interrelationship of each pathway during development and homeostasis are unclear. To precisely evaluate the relative contributions of DSB repair pathways during mammalian development, we compared the consequences of germ-line disruption of either HR or NHEJ. Unexpectedly, our data suggest a specific requirement for each pathway at distinct developmental stages during mammalian neurogenesis.

## Results

We evaluated the relative contribution of DNA DSB repair pathways during mammalian development. To study each DSB repair pathway, we used mice containing germ-line disruption of either *Xrcc2* or *Lig4*. To disrupt HR, we generated $Xrcc2^{-/-}$ mice by targeted deletion of exon 3 that encompasses ≈75% of the *Xrcc2* coding sequence. Xrcc2 is one of a number of mammalian homologues of *Saccharomyces cerevisae* Rad 51 and plays a critical nonredundant role in HR (11, 12). The $Xrcc2^{-/-}$ mice were embryonically lethal, and mouse embryonic fibroblasts (MEFs) derived from these mice were hypersensitive to DNA damaging agents and underwent spontaneous chromosomal rearrangements in culture (Fig. 6, which is published as supporting information on the PNAS web site). The early embryonic lethality and DNA damage sensitivity in our *Xrcc2* mutant is similar to another *Xrcc2* mutant (13, 14), and collectively, these data show that Xrcc2 is critical for the cellular response to DNA DSBs and for maintenance of genomic stability.

Despite the importance of HR, NHEJ is often considered the predominant pathway for repair of DNA DSBs (4). To further establish the roles for NHEJ and HR during development, we compared $Xrcc2^{-/-}$ mice (defective HR) with $Lig4^{-/-}$ mice (defective NHEJ). We found a striking difference in the spatiotemporal requirements for each DNA repair pathway during development. Inactivation of Xrcc2 affected early embryogenesis and resulted in abundant apoptosis of proliferating cells and resultant lethality around embryonic days 9–10 (E9–E10) (Fig. 1*A*). Some $Xrcc2^{-/-}$ embryos could be found at later times, and these *Xrcc2* knockout embryos also showed widespread apoptosis in proliferating forebrain and hindbrain structures (Fig. 1*B k–o*). In stark contrast, disruption of NHEJ resulting from Lig4 loss had no obvious consequences until developmental times later than E12, because no apoptosis above control levels (Fig. 1*B a–e*) was observed in $Lig4^{-/-}$ embryos before E12 (Fig. 1*B f–i*), suggesting that NHEJ is dispensable during a substantial and critical period of early- to mid-embryonic development.

Conflict of interest statement: No conflicts declared.

This paper was submitted directly (Track II) to the PNAS office.

Abbreviations: Atm, ataxia telangiectasia mutated; DSB, double-strand break; E*n*, embryonic day *n*; HR, homologous recombination; NHEJ, nonhomologous end-joining; P*n*, postnatal day *n*; SVZ, subventricular zone; VZ, ventricular zone.

‡To whom correspondence should be addressed at: Department of Genetics and Tumor Cell Biology, St. Jude Children's Research Hospital, 332 North Lauderdale, Memphis, TN 38105. E-mail: peter.mckinnon@stjude.org.

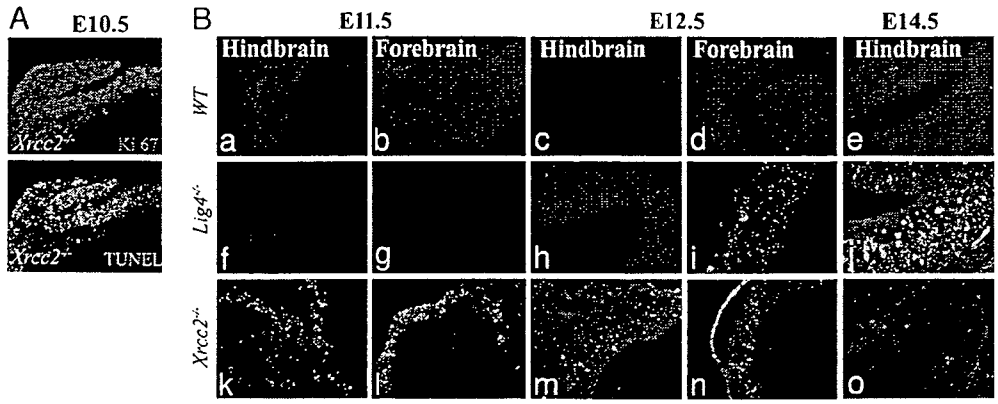


**Fig. 1.** Inactivation of NHEJ or HR affects different embryonic stages during mouse development. Widespread apoptosis can be found in the *Xrcc2*$^{-/-}$ embryo by E10.5 and is illustrated showing neuroepithelium and adjacent cephalic mesenchyme. (*A*) Ki67 immunoreactivity (red) marks proliferating cells, and TUNEL staining (green) identifies cells undergoing apoptosis. (*B*) Although apoptosis is widespread in the proliferative cells of the *Xrcc2*$^{-/-}$ embryo at E11.5, it is not detectable in WT or *Lig4*$^{-/-}$ embryos until E12.5. In the differentiating hindbrain region at E14.5, Lig4, but not Xrcc2, loss is associated with apoptosis. (Magnification: ×200.)

Because the above data indicate the importance of NHEJ from E12, a stage at which regional differentiation of the nervous system is occurring, we determined the respective requirements for NHEJ and HR at later stages of mammalian nervous system development, where there are clear demarcations between proliferating and differentiating tissues. Analysis of *Xrcc2*$^{-/-}$ and *Lig4*$^{-/-}$ E14.5 embryos highlighted the difference in the utilization of each DSB pathway during development and confirmed a particular requirement for Xrcc2 during proliferation. TUNEL-positive cells were located almost exclusively in the proliferative ventricular zone (VZ) of the *Xrcc2*$^{-/-}$ embryos (Fig. 2*A*). In contrast, apoptosis was largely localized to postmitotic cells of the subventricular zone (SVZ) in *Lig4*$^{-/-}$ embryos (Fig. 2*B*). However, apoptosis does occur in the VZ in *Lig4*$^{-/-}$ mice, albeit substantially less than the SVZ (Fig. 2*B*). There are two possibilities that could explain the occurrence of apoptotic cells in the VZ in E14 *Lig4*$^{-/-}$ mice. These cells could be differentiating but have not yet migrated, or these cells are proliferative even though proliferative cells at earlier stages of development are unaffected by Lig4 loss. To distinguish between these possibilities, we further analyzed the cellular identity of the apoptotic cells in the *Lig4*$^{-/-}$ VZ. We used an early neural differentiation marker, doublecortin (a microtubule-associated protein; see ref. 15), that could distinguish early cell-fate of some neural precursors present in the VZ (Fig. 2 *C* and *E*). To identify the nature of the cells undergoing apoptosis, we used double labeling with immunostaining for doublecortin and TUNEL for apoptosis. In the *Lig4*$^{-/-}$ embryos at E14, we found doublecortin-positive cells that were undergoing apoptosis, suggesting that many of the apoptotic cells in the VZ of the *Lig4*$^{-/-}$ embryos were differentiating and were not proliferative (Fig. 2 *F–H*). In contrast, we were unable to identify costaining cells in the VZ of the *Xrcc2*$^{-/-}$ embryos (Fig. 2 *I–K*). Thus, these data suggest that the apoptotic cells in the VZ of *Lig4*$^{-/-}$ embryos were undergoing differentiation.

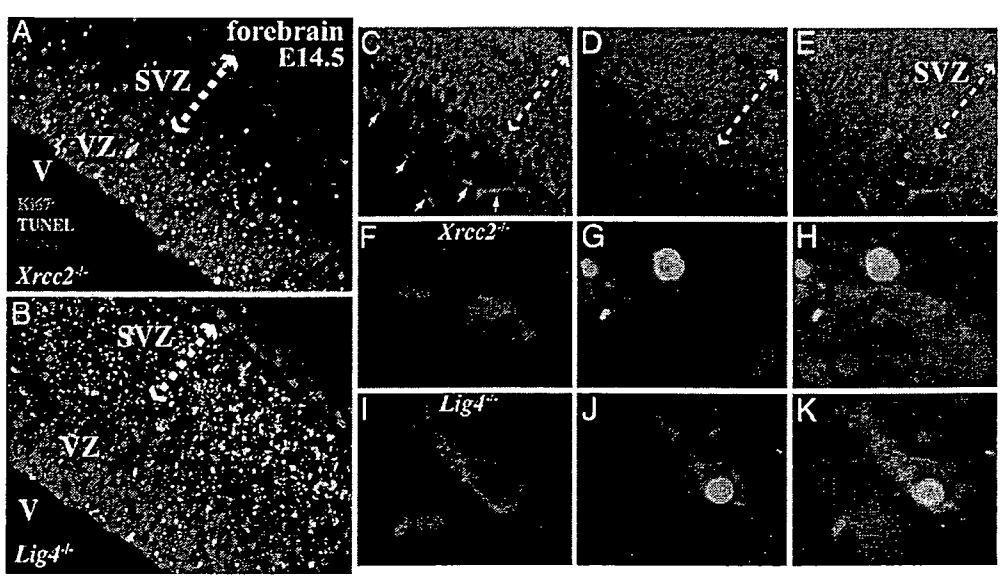


**Fig. 2.** Selective utilization of NHEJ and HR during development. At E14.5, apoptosis is found in the forebrain proliferative VZ of the *Xrcc2*$^{-/-}$ embryo, whereas in the *Lig4*$^{-/-}$ embryo, TUNEL-positive cells are predominantly located in the postmitotic SVZ (indicated by arrows). (*A* and *B*) Magnification: ×200; V, ventricle. (*C* and *E*) Doublecortin identifies scattered differentiating cells in the VZ. (*D* and *E*) DAPI staining shows the whole embryonic forebrain. (Magnification: ×200.) (*F–K*) TUNEL-positive cells did not colocalize with doublecortin-positive cells in *Xrcc2*$^{-/-}$ embryos (*F–H*) but did so in *Lig4*$^{-/-}$ embryos (*I–K*). (Magnification: ×1,000.)

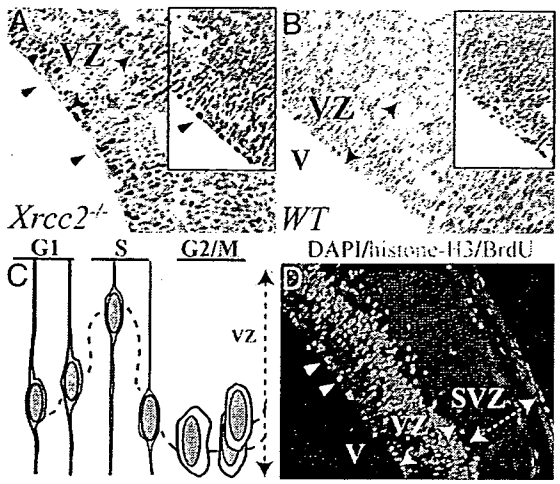


Fig. 3. The DNA damage response in $Xrcc2^{-/-}$ embryos occurs in $G_2$/M cells of the VZ. Xrcc2 deficiency leads to p53 ser18 phosphorylation (*A*) and p53 stabilization (*A Inset*) in a layer of cells at the margin (arrowheads) of the ventricle (V) of an E14.5 embryo. (*B*) No p53 phosphorylation or stabilization (*Inset*) is found in WT embryo. (*C*) The cartoon represents the characteristic position of the progenitor cell nucleus within the VZ as the cell cycle progresses. (*D*) Cells that are immunopositive for phosphorylated histone H3 staining (green signal) indicate cells in mitosis, and BrdU-positive cells (red signal) mark those in S phase (arrowheads). The VZ and the postmitotic SVZ are marked.

DNA damage in the developing nervous system resulting from dysfunctional NHEJ (*Lig4* or *Xrcc4* deletion) activates a pathway that is p53 dependent (16, 17). To determine the nature of the DNA damage response in the $Xrcc2^{-/-}$ embryos, we used immunostaining for phosphorylation of p53 ser18 (equivalent to human p53 ser15) to identify whether cells undergo DNA damage-induced p53 activation. We found p53 phosphorylation selectively occurred in the VZ, predominantly in a single row at the ventricular margin in $Xrcc2^{-/-}$ embryos (Fig. 3*A*), but not in WT littermate controls (Fig. 3*B*). This location is notable because the nucleus of proliferating cells within the VZ has a defined spatiotemporal relationship with the progression of the cell cycle (18), and, in this position, cells are in either second gap ($G_2$) or mitotic (M) (Fig. 3*C*). To confirm p53 activation in S phase was the case for $Xrcc2^{-/-}$ embryos, we used immunostaining for phosphorylated histone H3 to identify cells in mitosis and BrdU incorporation to mark cells in S phase. Cells immunopositive for antiphospho-histone H3 were clearly demarcated as a single cell layer in both the WT and $Xrcc2^{-/-}$ ventricular margin and coincided with p53 phosphorylation resulting from *Xrcc2* inactivation (Fig. 3*D*). BrdU also labels a band of S phase cells within the VZ superior to the p53-positive cells (Fig. 3*D*). The subsequent distribution of apoptotic cells away from the position of the p53 staining cells in the VZ (see Fig. 2*A*) most likely results from the failed commencement of another cell cycle. Additionally, some antiphospho-histone H3-positive mitotic cells were also present at the VZ/SVZ margin, indicating the occurrence of a laminar population that also coincide with scattered apoptotic cells in this region in $Xrcc2^{-/-}$ embryos (Fig. 2*A*). Therefore, despite a previous report of Xrcc2 loss leading to death in the SVZ (13, 14), our data now supports a requirement for HR solely in proliferating cells. Thus, activation of p53 in $G_2$/M cells in the $Xrcc2^{-/-}$ embryo reflects DNA damage signaling arising after DNA replication, at a time when HR would normally be available to facilitate DNA repair. Thus, there is a separate requirement for NHEJ and HR at different developmental stages and within different tissues during mouse nervous system development.

To further define the relationship between DNA damage signaling arising from defective NHEJ or HR, we used a genetic approach to determine the involvement of ataxia telangiectasia mutated (Atm), a protein kinase critical for the response to DNA DSBs) (19–22) or p53 in $Lig4^{-/-}$ or $Xrcc2^{-/-}$ embryos. Although Atm has been implicated in HR in *in vitro* studies (23–25), no data are available in the context of an *in vivo* setting. Importantly, no relationship between Atm and HR defects has been examined during mammalian development. However, in the case of $Lig4^{-/-}$, previous work has shown that both Atm and p53 are required for genotoxic stress-induced apoptosis in the $Lig4^{-/-}$ nervous system (17, 26–28). To assess whether a similar signaling scenario exists during neural development after HR inactivation, we generated $Xrcc2^{-/-}$ embryos with associated loss of either Atm or p53, by interbreeding either $Xrcc2^{+/-}p53^{+/-}$ or $Xrcc2^{+/-}Atm^{+/-}$ mice.

We found that Atm was required for apoptosis after inactivation of NHEJ but not for apoptosis resulting from disruption of HR (Fig. 4). Abundant apoptosis was found throughout the E14.5 $Lig4^{-/-}$ cortex that was dependent on Atm (Fig. 4*A*) and p53 (data not shown). In contrast to the difference between $Lig4^{-/-}$ and $Lig4^{-/-}Atm^{-/-}$ embryos, $Xrcc2^{-/-}Atm^{-/-}$ embryos showed similar apoptosis to $Xrcc2^{-/-}$ embryos (Fig. 4*A*). However, loss of p53 prevented apoptosis in $Xrcc2^{-/-}$ embryos (Fig. 4*A*). WT embryos showed little or no apoptosis, whereas apoptosis was markedly reduced in the $Xrcc2^{-/-}p53^{+/-}$ embryos (data not shown). Apoptosis present in the DNA repair mutants after introduction onto an $Atm^{-/-}$ background was quantified (Fig. 4*B*). Apoptosis levels in $Xrcc2^{-/-}$ embryos indicates that apoptosis resulting from HR dysfunction is confined to the VZ, and that there is no significant difference between apoptosis in $Xrcc2^{-/-}$ and $Xrcc2^{-/-}Atm^{-/-}$ ($P > 0.05$), whereas loss of Atm significantly reduced apoptosis after Lig4 loss ($P < 0.0001$). Thus, although Atm is required for neural apoptosis that occurs in the SVZ of $Lig4^{-/-}$ embryos, it is not required for that resulting from Xrcc2 loss.

Consistent with TUNEL analysis, lethality associated with $Xrcc2^{-/-}$ was p53 dependent because $Xrcc2^{-/-}p53^{+/-}$ and $Xrcc2^{-/-}p53^{-/-}$ mice were viable, although in both cases the mice were smaller and less robust than WT littermates (Fig. 4*C*). Again, in accord with TUNEL analysis, $Xrcc2^{-/-}Atm^{-/-}$ (and $Xrcc2^{-/-}Atm^{+/-}$) embryos were recovered at the same frequency as $Xrcc2^{-/-}$ embryos, further indicating that loss of Atm provided no survival advantage for $Xrcc2^{-/-}$ deficient embryos. As reported in refs. 26 and 27, *Lig4* inactivation is rescued by p53 or Atm deficiency, although $Lig4^{-/-}Atm^{-/-}$ mice do not survive past postnatal day 1 (P1).

We also used a biochemical approach to examine the connection between Atm and DNA damage after HR inactivation by determining Atm autophosphorylation in $Xrcc2^{-/-}$ and $Lig4^{-/-}$ neural tissue. Atm activation requires autophosphorylation of ser1981, and this event is rapidly induced after DNA DSBs (29). Therefore, we isolated developing brain from $Xrcc2^{-/-}$ or $Lig4^{-/-}$ E13.5 embryos and determined Atm activation by using an antibody that recognized phosphorylated ser1981 of Atm (ser1987 in mouse Atm). At E13.5, when there are substantial cellular consequences resulting from Xrcc2 loss, Atm phosphorylation was similar to WT levels. In contrast, at this same developmental stage, loss of Lig4 leads to Atm phosphorylation in developing neural tissues (Fig. 4*D*). The specificity of the antisera used is shown by an absence of immunoreactivity in $Atm^{-/-}$ developing brain after ionizing radiation exposure compared with robust phosphorylation in irradiated WT tissue (Fig. 4*D*). Qualitatively similar results were obtained at other developmental times (data not shown). Therefore, although DNA damage arising from dysfunction in HR in $Xrcc2^{-/-}$ embryos

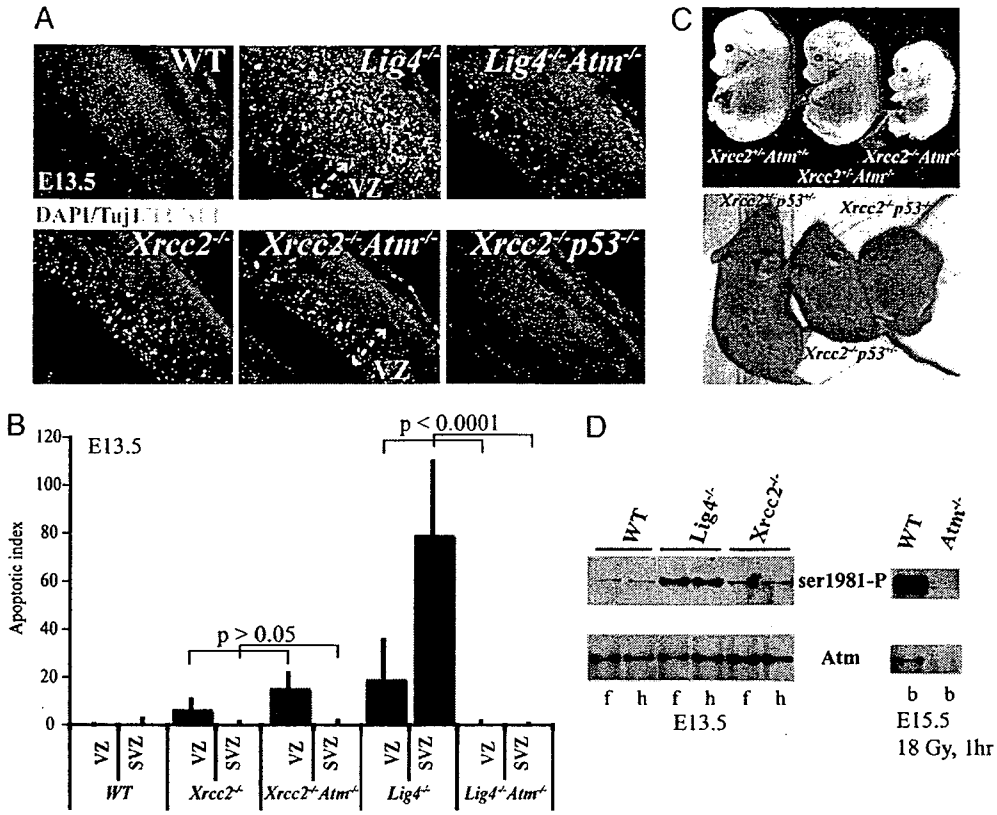


Fig. 4. Atm is not required for DNA damage signal transduction after Xrcc2 loss. (*A*) Analysis of apoptosis was done by using TUNEL staining in E14.5 using WT, $Lig4^{-/-}$, $Lig4^{-/-}Atm^{-/-}$, $Xrcc2^{-/-}$, $Xrcc2^{-/-}Atm^{-/-}$, and $Xrcc2^{-/-}p53^{-/-}$ embryos. Tuj1 immunostaining identifies the differentiating neural cell populations. The merged composites are an overlay of Tuj1, TUNEL, and DAPI staining. (*B*) The amount of apoptosis was quantified in the VZ and the SVZ of the E14.5 nervous system from the indicated mutants. (*C*) $Xrcc2^{-/-}$ mice can survive on a $p53^{-/-}$ or $p53^{+/-}$ background, whereas Atm loss confers no survival advantage. (*D*) Phosphorylation (ser1981) of Atm was found in developing brain tissue from $Lig4^{-/-}$ but not $Xrcc2^{-/-}$; f, forebrain; h, hindbrain isolated from E13.5. Specificity of the Atm antibodies is shown using WT and $Atm^{-/-}$ E15.5 embryonic brain (b) after ionizing radiation exposure.

presumably includes DNA DSBs, these DNA breaks do not activate Atm in the embryonic nervous system.

As p53 deficiency rescued the lethality of either $Xrcc2^{-/-}$ or $Lig4^{-/-}$ mice, we monitored these mice as they aged. Compared with the $Lig4^{-/-}p53^{-/-}$ mice, the $Xrcc2^{-/-}p53^{-/-}$ and $Lig4^{-/-}p53^{+/-}$ were substantially less robust and often died perinatally of undetermined causes. However, of the $Xrcc2^{-/-}p53^{-/-}$ mice that survived, all developed multiple tumor types. Tumor onset in $Xrcc2^{-/-}p53^{-/-}$ mice was rapid and with different tumor types present by 10 weeks of age (Fig. 5*A*). In contrast, $Lig4^{-/-}p53^{-/-}$ mice developed either pro-B cell lymphoma or medulloblastoma or both tumor types by 12 weeks of age (28, 30). Therefore the tumor spectrum in $Xrcc2^{-/-}p53^{-/-}$ mice was broader than that arising from Lig4 loss and included lymphoma, skin tumor, sarcoma (Fig. 5*B*), and, like $Lig4^{-/-}p53^{-/-}$ mice (28), medulloblastoma. Although $Xrcc2^{-/-}$p53$^{-/-}$ mice developed lymphomas, these tumors were B220 negative and therefore distinct to the pro-B cell lymphoma (B220+) present in $Lig4^{-/-}p53^{-/-}$ mice (data not shown). CD4/CD8 immunophenotyping of $Xrcc2^{-/-}p53^{-/-}$ lymphomas showed CD8+/CD4− immunoreactivity indicative of a thymoma (Fig. 5*C*). Spectral karyotyping of primary thymomas from $Xrcc2^{-/-}p53^{-/-}$ showed multiple chromosomal rearrangements (Fig. 5*D*, boxed). However, unlike the $Lig4^{-/-}p53^{-/-}$ pro-B cell lymphomas that are characterized by an IgH-MYC-C t (12, 15) translocation (Fig. 5*D Inset*), no recurring chromosomal rearrangements were found between different primary $Xrcc2^{-/-}p53^{-/-}$ tumors. Moreover, flow cytometry analysis of thymocytes and spleenocytes from $Xrcc2^{-/-}$p53$^{-/-}$ mice by using CD4, CD8, IgM, and B220 cell surface markers showed similar mature B and T cell populations to those of age-matched WT controls, indicating that, in contrast to Lig4 inactivation, the gross development of B and T cells was unaffected by Xrcc2 deficiency (data not shown). Although $Lig4^{+/-}p53^{-/-}$ are prone to sarcomas (31), $Lig4^{-/-}p53^{+/-}$ mice do not develop tumors, at least until their death at ≈6 months (data not shown). In contrast to $Lig4^{-/-}$, $Xrcc2^{-/-}p53^{+/-}$ mice were extremely cancer prone because thymoma could be found before 12 weeks of age (Fig. 5*A*). Despite the cancer proneness of $Xrcc2^{-/-}$ mice, there was no evidence for Xrcc2 haploinsufficiency as $Xrcc2^{+/-}p53^{-/-}$ mice developed tumors in a manner indistinguishable from $p53^{-/-}$ mice (Fig. 5*A*).

## Discussion

Here we have shown that, during mammalian nervous system development, the two major DNA DSB repair pathways, NHEJ and HR, function in a more regional and nonoverlapping manner than previously appreciated. This spatiotemporal distinction also reflects a differential requirement for DNA damage signal transducers and in the tumor spectrum resulting from disruption of either pathway. Our data suggest that HR is the operative DNA DSB repair pathway during early mammalian development and may explain why NHEJ does not appear to be functionally important until around midgestation. Because cellular differentiation will preclude the availability of suitable homologous templates for HR (i.e., sister

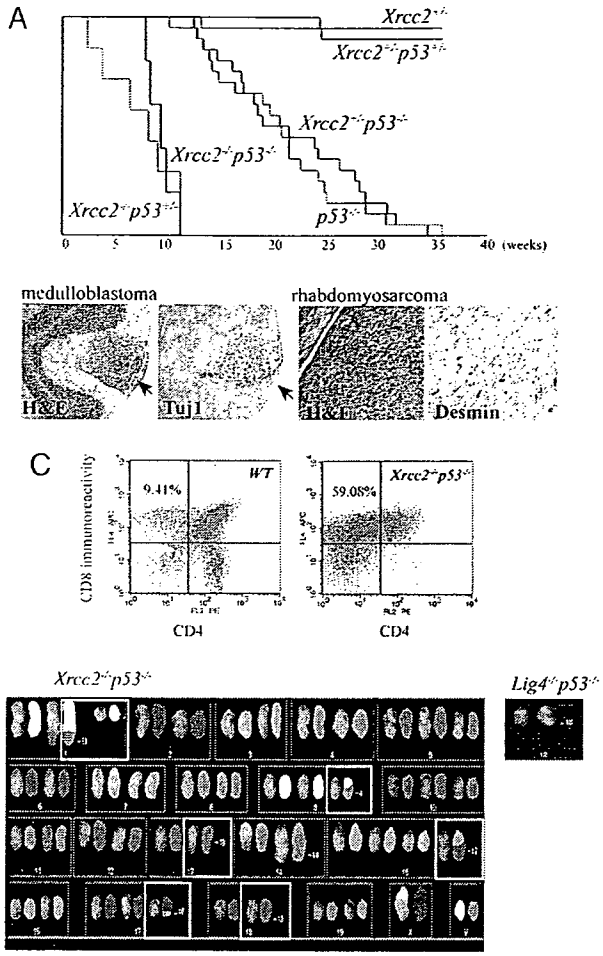


Fig. 5. Inactivation of HR results in multiple tumor types. (*A*) A Kaplan–Meier curve shows survival of mice with various combinations of *Xrcc2* and *p53* mutant alleles and also shows $Xrcc2^{+/-}$ is not haploinsufficient for tumors as $Xrcc2^{+/-}p53^{-/-}$ mice developed tumors of the same kind and at the same rate as $p53^{-/-}$ littermates. (*B*) A medulloblastoma staining immunopositive for the neuronal marker Tuj1 and a sarcoma staining immunopositive for desmin were isolated from a 10-week-old $Xrcc2^{-/-}p53^{-/-}$ mouse. Arrows indicate the medulloblastoma within the cerebellar molecular layer. (*C*) Lymphomas from $Xrcc2^{-/-}p53^{-/-}$ mice were CD8-immunopositive, indicative of a thymoma. Spectral karyotyping reveals a number of chromosomal rearrangements from a primary $Xrcc2^{-/-}p53^{-/-}$ thymoma. (*D*) Image shows the spectral color image on the left and the pseudocolor chromosome on the right. (*D Inset*) Spectral karyotyping (SKY) analysis from a pro-B cell lymphoma from $Lig4^{-/-}p53^{-/-}$ mice showing a typical translocation involving t (12, 15) that affects IgH and c-Myc.

chromatids), NHEJ becomes a main repair pathway. These data are consistent with lower eukaryotes such as yeast in which the driving cellular process is proliferation, and DNA repair occurs predominantly via HR (1, 4). The usage of HR during this early development would also ensure the greatest chance of error-free repair, thus maintaining embryonic genomic fidelity.

Our finding that inactivation of HR leads to profound defects exclusively in proliferating neural cells clearly contrasts another description of Xrcc2 loss, where it was reported that substantial apoptosis occurred in postmitotic neural cells (14). In reconciling that conclusion with our current data, it seems likely that, in the earlier report, the affected cells were the phospho-H3- or BrdU-positive proliferative cells located at the VZ/SVZ border and not postmitotic neurons (see Fig. 3*D*). A striking difference between the inactivation of each DSB repair pathway was the absence of obvious defects after Lig4 loss until almost midway through development. Whereas loss of NHEJ leads to a pronounced wave of apoptosis from E12.5 in differentiating and migrating neural cells, we nonetheless also found apoptosis in the VZ where proliferative cells reside. However, many of these TUNEL-positive cells in the VZ colocalized with doublecortin, suggesting the presence of differentiated cells within the VZ area. It is also possible that in $Lig4^{-/-}$ embryos the effects seen in the VZ may be an indirect effect of the substantial apoptosis in the SVZ, or alternatively, they may in some cases be proliferating cells and reflect the fact that NHEJ can be operative during all phases of the cell cycle (7, 9).

The abundant apoptosis in differentiating cells resulting from failure of NHEJ suggests that this pathway is required to address DNA damage present after cell cycle exit, perhaps arising from incomplete repair via HR, and so may therefore act as an additional and final genomic surveillance as cells differentiate and mature. Alternatively, NHEJ may be required for new DNA damage that occurs from cellular metabolism such as free radical damage arising from oxidative stress (32), rather than to address DNA lesions not repaired via HR.

The lack of an observable effect of Atm deficiency in $Xrcc2^{-/-}$ embryos was unexpected, given the reported link to HR (23–25) and the importance of Atm in the DSB response (19–22). This finding implies that Atm is not integral for HR in all settings and may be important for HR in only some tissues, or at later stages of development. In fact the Atm-related protein, ATR, has been implicated in HR and proliferation (33, 34), and may therefore be primarily involved in DSB signaling (e.g., to p53) (35) in the VZ during development.

We also observed a difference in the tumor spectrum resulting from inactivation of each DNA DSB repair pathway. The broader spectrum of tumors present in the $Xrcc2^{-/-}$ animals probably reflects the particular requirement for HR during DNA replication of precursor or stem cells. The one common tumor type, medulloblastoma, that results from loss of either Lig4 or Xrcc2, reflects postnatal development of the cerebellum via generation of granule neurons from an outer proliferative layer (36) where Xrcc2 is functionally important, and a postmitotic differentiating migratory layer where Lig4 is functionally important. Thus, both proliferative precursors and differentiating neurons are present in this organ, and the maintenance of genomic integrity requires the respective contributions of both HR and NHEJ to prevent medulloblastoma.

In summary, we have shown that the two major DNA DSB repair pathways function in a coordinated manner during development, although there is a defined spatiotemporal distinction in the functional importance of each repair pathway during neurogenesis. Therefore, together, these two pathways effectively maintain genomic integrity and suppress genotoxic stress via cooperative, but largely nonoverlapping, roles during mammalian development.

## Materials and Methods

**Mice.** *Xrcc2* was inactivated in the mouse germ line by deletion of exon 3, which contains >75% of the ORF. Full details of the generation of *Xrcc2* null mice are available in *Supporting Materials and Methods*, which is published as supporting information on the PNAS web site. $Xrcc2^{-/-}p53^{-/-}$ and $Xrcc2^{-/-}p53^{+/-}$ mice were obtained by intercrossing of $Xrcc2^{+/-}p53^{+/-}$ animals. $Xrcc2^{-/-}Atm^{-/-}$ mice were obtained by intercrossing of $Xrcc2^{+/-}Atm^{+/-}$ animals. $Lig4^{-/-}p53^{-/-}$ or $Lig4^{-/-}Atm^{-/-}$ mice used in this study have been described (26, 28). The presence of a vaginal plug was designated as E0.5 and the day of birth as P0. All animals were housed in an American Association for the Accreditation of Laboratory Animal Care accredited facility and were maintained in accordance with the National Institutes of Health *Guide for the Care and Use of Laboratory Animals*. The institutional animal care and use committee at St. Jude

Children's Research Hospital approved all procedures for animal use.

**Histological Analysis.** Embryos were fixed in 4% paraformaldehyde, cryoprotected in 25% sucrose/PBS, and cryosectioned (10-$\mu$m sagittal sections) by using an HM500 M cryostat (Microm International GmbH, Walldorf, Germany), whereas tissues were fixed in 10% buffered formalin, embedded in paraffin, and sectioned (7-$\mu$m sagittal sections) by using an HM325 microtome (Microm International GmbH). These sections were stained with hematoxylin and eosin according to standard procedures. Immunohistological analyses of tissue were performed by using the following antibodies: anti-p53 (CM5; 1:500; NovoCastra); anti-p53 phospho-ser15 (1:100; Cell Signaling Technology, Beverly, MA); antiactive caspase 3 (1:500; BD Biosciences); antiphospho-histone H3 (ser10) (6G3; 1:1,000; Cell Signaling Technology); anti-proliferating cell nuclear antigen (1:100; Calbiochem); anti-Ki67 (1:1,000; NovoCastra); anti-$\beta$-tubulin III (Tuj1; 1:1,000; Babco, Richmond, CA); antidesmin (1:500; DAKO); antidoublecortin (1:1,000; Abcam, Inc., Cambridge, MA); and anti-CD4, anti-CD8, and anti-B220 (all were used at 1:50; PharMingen). Antigen retrieval was used for all antibodies, except cell surface markers. Sections were incubated with antibodies overnight after quenching endogenous peroxidase by using 0.6% hydrogen peroxide, and immunoreactivity was visualized with the VIP peroxidase substrate kit (Vector Laboratories) according to the manufacturer's directions after the tissues were treated with biotinylated secondary antibody and avidin DH-biotinylated horseradish peroxidase-H complex (Vectastain elite kit; Vector Laboratories). Sections were counterstained with 0.1% methyl green (Vector Laboratories), dehydrated, and mounted in DPX (BDH). For fluorescence signals, FITC or indocarbocyanine (Cy3) conjugated secondary antibody (Jackson ImmunoResearch) was used. DAPI (4′,6-diamidino-2-phenylindole) staining was used for counterstaining. Apoptosis was measured by using Apoptag (Chemicon). Quantitative analyses of TUNEL-positive cells in the embryonic forebrain were obtained by using IMAGE PROCESSING TOOL KIT V5.0 (Reindeer Graphics, Asheville, NC) by using three to five embryos at E13.5 for each genotype. S phase cells were visualized after a 60-min pulse of BrdU (100 $\mu$g/g body weight delivered i.p. at E14.5). BrdU incorporation was visualized by using a rat monoclonal anti-BrdU (Abcam, Inc.) after sections were treated with SSC solution for 2 h at 65°C and then 30 min in 2 M HCl at 37°C and rinsed in 0.1 M boric acid (pH 8.5) followed by routine immunohistochemistry. Spectral karyotyping (SKY) was done by using a SKY probe from Applied Spectral Imaging (Vista, CA) with a single cell suspension of primary lymphoma enriched for metaphases after a 4.5-h colcemid incubation. Applied Spectral Imaging protocols were followed for hybridization and detection.

**Atm Phosphorylation Analysis.** Atm was immunoprecipitated from microdissected E13.5 embryonic brain regions with Atm antibody D1611 (obtained from Dr. Michael Kastan, St. Jude Children's Research Hospital, Memphis, TN) by using protein A/G agarose beads. Tissue lysates for immunoprecipitation were prepared in 50 mM Tris (pH 7.5) containing 150 mM NaCl, 50 mM NaF, 1% Tween 20, 0.2% Nonidet P-40, 1 mM 4-(2-aminoethyl)benzenesulfonyl fluoride (Roche), 1 mM DTT, and 1× protease inhibitor mixture (Roche). Beads were rinsed with RIPA buffer (0.15 mM NaCl/0.05 mM Tris·HCl, pH 7.2/1% Triton X-100/1% sodium deoxycholate/0.1% SDS), split 1:2, run on two separate 3–8% NOVEX (San Diego) Tris-acetate gels, and electroblotted to poly(vinylidene difluoride) (PVDF) membranes. Phosphorylated Atm was visualized by using anti-ser1981 Atm antibody (Rockland Immunochemicals), whereas MAT3 antibody (obtained from Dr. Yosef Shiloh, Tel Aviv University, Tel Aviv) was used to detect total Atm. Two separate sets of embryos were used to determine Atm phosphorylation status.

**Flow Cytometry Analysis.** Immunophenotyping of tumor cell suspensions was done as described (26) by using CD4, CD8, B220, and IgM antibodies obtained from PharMingen.

We thank Suzanne Baker, Gerard Grosveld, and Michael Kastan for discussions and comments on the manuscript. We also thank the Hartwell Center, the Cancer Center Cytogenetics Core, and the Transgenic Core facility at St. Jude Children's Research Hospital for their support of this work. These studies were supported by National Institutes of Health Grants NS-37956 and CA-21765, Cancer Center Support Grant P30 CA21765, and the American Lebanese and Syrian Associated Charities (ALSAC) of St. Jude Children's Research Hospital.

1. West, S. C. (2003) *Nat. Rev Mol. Cell Biol.* **4**, 435–445.
2. Thompson, L. H. & Schild, D. (2001) *Mutat. Res.* **477**, 131–153.
3. Mills, K. D., Ferguson, D. O. & Alt, F. W. (2003) *Immunol. Rev.* **194**, 77–95.
4. Lieber, M. R., Ma, Y., Pannicke, U. & Schwarz, K. (2003) *Nat. Rev. Mol. Cell Biol.* **4**, 712–720.
5. Ahnesorg, P., Smith, P. & Jackson, S. P. (2006) *Cell* **124**, 301–313.
6. Buck, D., Malivert, L., de Chasseval, R., Barraud, A., Fondaneche, M. C., Sanal, O., Plebani, A., Stephan, J. L., Hufnagel, M., le Deist, F., *et al.* (2006) *Cell* **124**, 287–299.
7. Rothkamm, K., Kruger, I., Thompson, L. H. & Lobrich, M. (2003) *Mol. Cell. Biol.* **23**, 5706–5715.
8. Couedel, C., Mills, K. D., Barchi, M., Shen, L., Olshen, A., Johnson, R. D., Nussenzweig, A., Essers, J., Kanaar, R., Li, G. C., *et al.* (2004) *Genes Dev.* **18**, 1293–1304.
9. Mills, K. D., Ferguson, D. O., Essers, J., Eckersdorff, M., Kanaar, R. & Alt, F. W. (2004) *Genes Dev.* **18**, 1283–1292.
10. Richardson, C. & Jasin, M. (2000) *Mol. Cell. Biol.* **20**, 9068–9075.
11. Johnson, R. D., Liu, N. & Jasin, M. (1999) *Nature* **401**, 397–399.
12. Griffin, C. S., Simpson, P. J., Wilson, C. R. & Thacker, J. (2000) *Nat. Cell Biol.* **2**, 757–761.
13. Deans, B., Griffin, C. S., O'Regan, P., Jasin, M. & Thacker, J. (2003) *Cancer Res.* **63**, 8181–8187.
14. Deans, B., Griffin, C. S., Maconochie, M. & Thacker, J. (2000) *EMBO J.* **19**, 6675–6685.
15. Gleeson, J. G., Allen, K. M., Fox, J. W., Lamperti, E. D., Berkovic, S., Scheffer, I., Cooper, E. C., Dobyns, W. B., Minnerath, S. R., Ross, M. E. & Walsh, C. A. (1998) *Cell* **92**, 63–72.
16. Abner, C. W. & McKinnon, P. J. (2004) *DNA Repair (Amst.)* **3**, 1141–1147.
17. Frank, K. M., Sharpless, N. E., Gao, Y., Sekiguchi, J. M., Ferguson, D. O., Zhu, C., Manis, J. P., Horner, J., DePinho, R. A. & Alt, F. W. (2000) *Mol. Cell* **5**, 993–1002.
18. Chan, W. Y., Lorke, D. E., Tiu, S. C. & Yew, D. T. (2002) *Anat. Rec.* **267**, 261–276.
19. Bakkenist, C. J. & Kastan, M. B. (2004) *Cell* **118**, 9–17.
20. Lavin, M. F., Birrell, G., Chen, P., Kozlov, S., Scott, S. & Gueven, N. (2005) *Mutat. Res.* **569**, 123–132.
21. McKinnon, P. J. (2004) *EMBO Rep.* **5**, 772–776.
22. Shiloh, Y. (2003) *Nat. Rev. Cancer* **3**, 155–168.
23. Bolderson, E., Scorah, J., Helleday, T., Smythe, C. & Meuth, M. (2004) *Hum. Mol. Genet.* **13**, 2937–2945.
24. Golding, S. E., Rosenberg, E., Khalil, A., McEwen, A., Holmes, M., Neill, S., Povirk, L. F. & Valerie, K. (2004) *J. Biol. Chem.* **279**, 15402–15410.
25. Morrison, C., Sonoda, E., Takao, N., Shinohara, A., Yamamoto, K. & Takeda, S. (2000) *EMBO J.* **19**, 463–471.
26. Lee, Y., Barnes, D. E., Lindahl, T. & McKinnon, P. J. (2000) *Genes Dev.* **14**, 2576–2580.
27. Sekiguchi, J., Ferguson, D. O., Chen, H. T., Yang, E. M., Earle, J., Frank, K., Whitlow, S., Gu, Y., Xu, Y., Nussenzweig, A. & Alt, F. W. (2001) *Proc. Natl. Acad. Sci. USA* **98**, 3243–3248.
28. Lee, Y. & McKinnon, P. J. (2002) *Cancer Res.* **62**, 6395–6399.
29. Bakkenist, C. J. & Kastan, M. B. (2003) *Nature* **421**, 499–506.
30. Gao, Y., Ferguson, D. O., Xie, W., Manis, J. P., Sekiguchi, J., Frank, K. M., Chaudhuri, J., Horner, J., DePinho, R. A. & Alt, F. W. (2000) *Nature* **404**, 897–900.
31. Sharpless, N. E., Ferguson, D. O., O'Hagan, R. C., Castrillon, D. H., Lee, C., Farazi, P. A., Alson, S., Fleming, J., Morton, C. C., Frank, K., *et al.* (2001) *Mol. Cell* **8**, 1187–1196.
32. Karanjawala, Z. E., Murphy, N., Hinton, D. R., Hsieh, C. L. & Lieber, M. R. (2002) *Curr. Biol.* **12**, 397–402.
33. Brown, E. J. & Baltimore, D. (2003) *Genes Dev.* **17**, 615–628.
34. Wang, H., Powell, S. N., Iliakis, G. & Wang, Y. (2004) *Cancer Res.* **64**, 7139–7143.
35. Tibbetts, R. S., Brumbaugh, K. M., Williams, J. M., Sarkaria, J. N., Cliby, W. A., Shieh, S. Y., Taya, Y., Prives, C. & Abraham, R. T. (1999) *Genes Dev.* **13**, 152–157.
36. Goldowitz, D. & Hamre, K. (1998) *Trends Neurosci.* **21**, 375–382.

American Journal of Medical Genetics Part A 143A:742–745 (2007)

*Clinical Report*

# Epstein–Barr Virus-Associated B-cell Lymphoma in a Patient With DNA Ligase IV (LIG4) Syndrome

**Nariaki Toita,[1]* Norikazu Hatano,[1] Satoru Ono,[1] Masafumi Yamada,[1] Ryoji Kobayashi,[1] Ichiro Kobayashi,[1,7] Nobuaki Kawamura,[1] Motohiko Okano,[1] Akira Satoh,[2] Atsuko Nakagawa,[3] Koichi Ohshima,[4] Masanobu Shindoh,[5] Tsuyoshi Takami,[6] Kunihiko Kobayashi,[1] and Tadashi Ariga[1]**

[1]Department of Pediatrics, Graduate School of Medicine, Hokkaido University, Sapporo, Japan
[2]Department of Oral Pathobiological Science, Graduate School of Dental Medicine, Hokkaido University, Sapporo, Japan
[3]Second Department of Pathology, Aichi Medical University, Nagakute, Japan
[4]Department of Pathology, School of Medicine, Fukuoka University, Fukuoka, Japan
[5]Department of Oral Pathology, Graduate School of Dental Medicine, Hokkaido University, Sapporo, Japan
[6]Department of Second Pathology, Gifu University School of Medicine, Gifu, Japan
[7]Department of Pediatrics, Kitami Red Cross General Hospital, Kitami, Japan

Received 7 September 2006; Accepted 24 November 2006

A 14-year-old Japanese girl with a progressing combined immunodeficiency had developed non-Hodgkin's diffuse large B cell lymphoma. Her molecular analysis showed a compound heterozygote of novel mutations in the *LIG4* gene, M249V substitution and a five nucleotides deletion from nucleotide position 1,270–1,274. She had also a set of characteristic clinical features of LIG4 syndrome. Mutations in the *LIG4* gene, which plays a critical role in the repair of DNA double-strand breaks, imply a correlation with malignancies and several cases with leukemia or lymphoma have already been reported. We report here on a case of LIG4 syndrome complicated with distinct EBV-associated B-cell lymphoma. © 2007 Wiley-Liss, Inc.

**Key words:** LIG4 syndrome; DNA ligase IV; immunodeficiency; EBV; lymphoma

**How to cite this article: Toita N, Hatano N, Ono S, Yamada M, Kobayashi R, Kobayashi I, Kawamura N, Okano M, Satoh A, Nakagawa A, Ohshima K, Shindoh M, Takami T, Kobayashi K, Ariga T. 2007. Epstein–Barr virus-associated B-cell lymphoma in a patient with DNA ligase IV (LIG4) syndrome. Am J Med Genet Part A 143A:742–745.**

## INTRODUCTION

DNA ligase IV (LIG4) syndrome (OMIM #606593) is a rare autosomal recessive disorder arising from mutations in the DNA ligase IV gene, which plays a critical role in the repair of DNA double-strand breaks by non-homologous end-joining mechanism [Riballo et al., 1999; O'Driscoll et al., 2001]. It is characterized by chromosomal instability, immunodeficiency, and developmental delay. Out of 11 previously reported patients, two cases with T cell leukemia, one case with B-cell lymphoma and one case with myelodysplasia have been reported, suggesting an increased risk for lymphoid malignancies in this disorder [Riballo et al., 1999; O'Driscoll et al., 2001; Ben-Omram et al., 2005; Buck et al., 2006; Enders et al., 2006; van der Burg et al., 2006]. In addition, a possible correlation between polymorphisms in the *LIG4* gene and a risk for malignancies such as breast cancer and multiple myeloma has been suggested [Goode et al., 2002; Roddam et al., 2002]. We present here a case of LIG4 syndrome complicated with Epstein–Barr virus (EBV)-associated large B-cell lymphoma.

Grant sponsor: Ministry of Education, Culture, Sports, Science and Technology; Grant numbers: 14370237, 14570714; Grant sponsor: Ministry of Health, Labor and Welfare; Grant number: 25060018-15.

*Correspondence to: Nariaki Toita, M.D., Department of Pediatrics, Graduate School of Medicine, Hokkaido University, North-15 west-7, Kita-ku, Sapporo, Japan. E-mail: toita@med.hokudai.ac.jp

DOI 10.1002/ajmg.a.31644

## MATERIALS AND METHODS

### Patient

A 14-year-old Japanese girl was admitted to Hokkaido University Hospital because of progressive gingival swelling and high fever. Her underlying clinical and laboratory features have already been precisely reported [Yamada et al., 2001]. Briefly, she had polydactyly, proportional microcephaly, short stature, and progressively decreasing serum levels of IgG and IgM, and the numbers of both peripheral B and T cells. Her skin fibroblast showed both spontaneous chromosome aberration and ionizing irradiation hypersensitivity but not mitomycin C hypersensitivity. Her clinical features including microcephaly, immunodeficiency and radiosensitivity resembled that of Nijmegen breakage syndrome (NBS) other than Bloom syndrome, Fanconi anemia, ataxia telangiectasia, and radiosensitive SCID (Artemis deficiency). However, no mutation was found in the coding lesion of *NBS1*. As well, a normal level of NBS1 protein was expressed in her fibroblast. She had been protected from severe infections by monthly intravenous immunoglobulin replacement therapy.

On admission, she had a whitely coated tumor involving her left upper gingiva and hard palate without apparent lymphadenopathy or hepatosplenomegaly. Laboratory findings were as followings; white blood cell count $1.5 \times 10^9$/L with 66% of neutrophils and 11% of lymphocytes, hemoglobin 97 g/L, platelet count $38 \times 10^9$/L, and C-reactive protein 26.3 mg/L. Flow-cytometry analysis of her peripheral blood mononuclear cells showed decreased numbers of both T ($CD3^+$, 33.1%) and B cells ($CD20^+$, 0.1%). T2-weighted magnetic resonance imaging showed a mixed intensity mass in the left maxillary sinus. The histopathological diagnosis was made as non-Hodgkin's diffuse large B cell lymphoma.

No abnormal cells were detected in either her peripheral blood or bone marrow. She was treated with the combination of reduced amounts of vincristine, cyclophosphamide, and prednisolone. Following this, erythematous desquamation of the skin, severe diarrhea, and severe persistent neutropenia developed. Finally, serious pulmonary aspergillosis developed despite anti-fungal therapy. She died of respiratory failure after four months of hospitalization. An autopsy was not performed.

### Histopathology

Tissue sample from the left maxillary sinus was fixed in 10% buffered formalin, embedded in paraffin, and stained with H&E. immunostains for CD3, CD20/L26, CD79a (DAKO, Kyoto, Japan) were performed for phenotypic analysis of the proliferating lymphocytes. Detection of EBV was done by immunostains for latent membrane protein (LMP-1) and EBV-determined nuclear antigen 2 (EBNA2) (DAKO) and by in situ hybridization with an oligoprobe for EBV-encoded small non-polyadenylated RNAs (EBER) and with a sense probe (negative control) [Weiss et al., 1992].

### DNA Sequencing

Genomic DNA was extracted from both peripheral blood neutrophils and skin fibroblasts. Overlapping fragments of the coding lesions of *LIG4* were amplified by polymerase chain reaction (PCR; 35 cycles of 94°C for 30 sec, 60°C for 30 sec, and 72°C for 1 min) with primers according to the previous report [O'Driscoll et al., 2001]. PCR products were supplied for direct sequencing reaction. Both PCR amplification and sequencing reaction were performed by GeneAmp PCR System 2400 (Perkin Elmer, Foster City, CA). Sequencing analyses were performed by ABI PRISM Gene Analyzer 310 (Perkin Elmer).

## RESULTS

### Histopathological Findings

Immunohistochemistry of the tumor cells demonstrated positive for both CD20 and CD79a but negative for CD3, and was histopathologically diagnosed as diffuse large B cell lymphoma (Fig. 1). Clonal immunoglobulin heavy chain gene rearrangement was noted by PCR analysis, suggesting monoclonal proliferation of the tumor cells. Although no EBV genome was demonstrated by semi-quantitative PCR analysis in her peripheral circulation, tumor cells were positive for EBV-encoded RNAs (EBERs), latent membrane protein-1, and EBV-determined nuclear antigen 2, indicating EBV-related type III latency [Okano and Gross, 2000].

### Sequencing Analysis and Immunoblot Analysis

We detected novel mutations, a five nucleotide deletion from 1,270 to 1,274 and an 745A > G substitution of the *LIG4* gene, which result in a frame shift at the amino acid position 424 and M249V amino acid substitution, respectively (Fig. 2). Compound heterozygosity was confirmed by sequencing analyses of both cloned DNA from the patient and DNA from her parents. The small deletion was inherited from her mother and the point mutation was identified in her father (data not shown). Western blot analysis revealed reduced LIG4 protein levels in her fibroblasts using monoclonal antibody for LIG4 (purchased from Santa Cruz Biotechnology, Santa Cruz, CA), compared with control cells (data not shown).

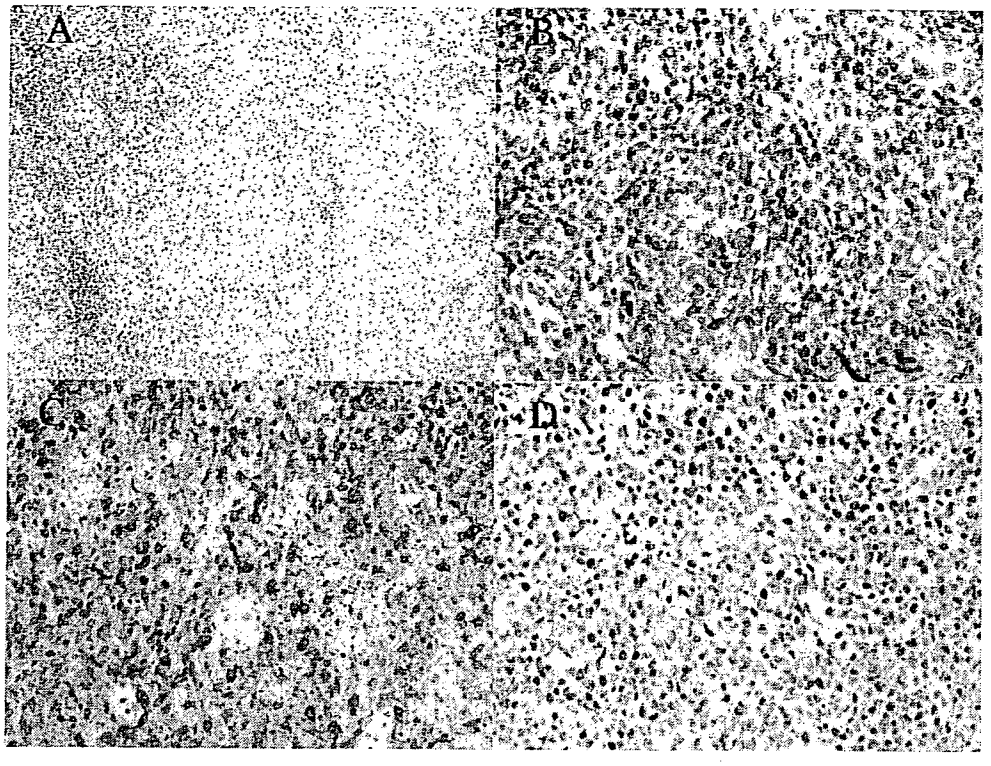


FIG. 1. Histopathology of the tumor. Tumor section was stained with hematoxylin-eosin (**A**; original × 100). Tumor cells are positive for CD79a (**B**; original × 400) and latent membrane protein-1 (**C**; original × 400) by immunohistochemistry. In situ hybridization study demonstrated EBV-encoded RNAs in the tumor cells (**D**; original × 400). [Color figure can be viewed in the online issue, which is available at www.interscience.wiley.com.]

## DISCUSSION

Here we describe a case of LIG4 syndrome complicated with distinct EBV-associated B-cell lymphoma, who had many phenotypic characteristics resembling NBS. O'Driscoll et al. [2001] screened NBS-like patients who had no mutations in *NBS1* and produced normal levels of nibrin, then identified several patients with mutations in *LIG4*. We also identified two novel mutations in the *LIG4* gene, a five-nucleotides deletion and M249V substitution. The small deletion result in a frame shift and its product lacking C-terminal XRCC4 binding site could be non-functional [Grawunder et al., 1998]. Methionine at amino acid 249 is located near an ATP-binding site and is conserved among other DNA

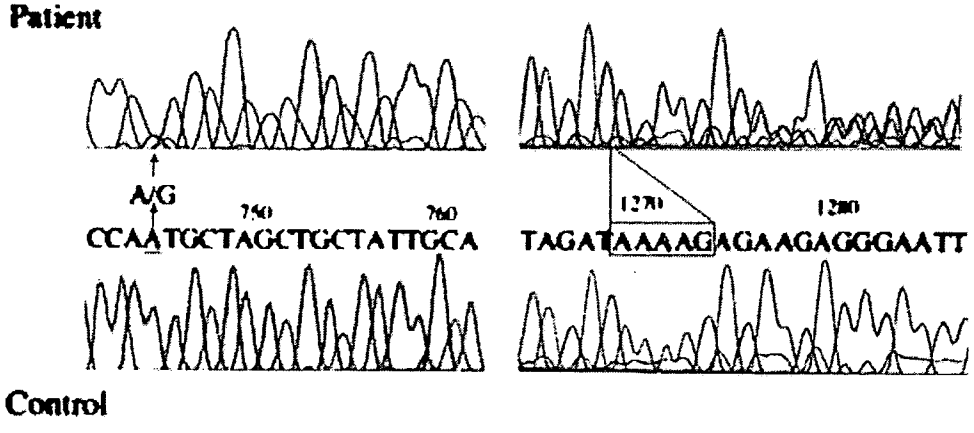


FIG. 2. Direct sequencing analysis demonstrates mutations in *LIG4*. The sequence of DNA from the patient shows heterozygote of 745A and 745G (**left upper panel**). A five nucleotides deletion from nucleotide position 1,270–1,274 (AAAAG) results in frame shift (**right upper panel**). Each mutation was detected on a different allele by sequencing analyses of cloned DNAs (data not shown). **Lower panels** show the sequence of DNA from a normal individual. [Color figure can be viewed in the online issue, which is available at www.interscience.wiley.com.]